Article

Current Biology

Drift of positional identity drives reproductive aging in a long-lived regenerative animal

Graphical abstract

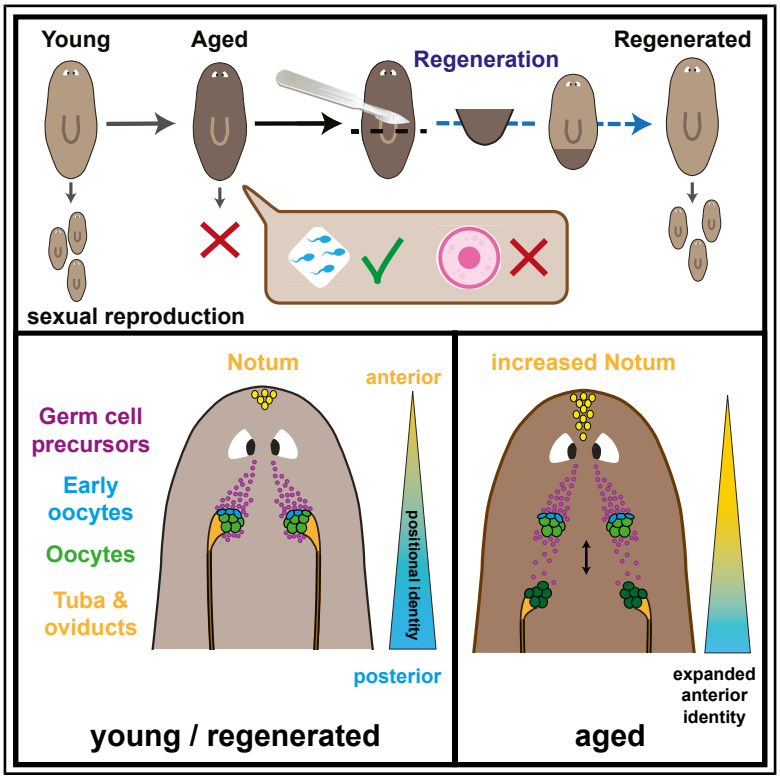

Authors

Andrew Verdesca, Axel Poulet, Maxwell Bales, Josien C. van Wolfswinkel

Correspondence

josien.van.wolfswinkel@yale.edu

In brief

Verdesca et al. find that planarians are long-lived but lose fertility with age due to changes in positional identity and gradual disorganization of the female germline. Resetting positional information by regeneration or alteration of Wnt signaling promotes fertility and may provide novel avenues to extend tissue health throughout organismal life.

Highlights

- Planarians lose fertility with age and regain it by regeneration
- Aged planarians develop ectopic ovaries with incomplete accessory structures
- Age-related changes in positional identity cause ovarian disorganization
- Modulation of Wnt-mediated positional information can extend fertility

Verdesca et al., 2026, Current Biology *36*, 1737–1747
April 6, 2026
https://doi.org/10.1016/j.cub.2026.02.050

CellPress

Current Biology

CellPress
OPEN ACCESS

Article

Drift of positional identity drives reproductive aging in a long-lived regenerative animal

Andrew Verdesca,[1,4] Axel Poulet,[1] Maxwell Bales,[1] and Josien C. van Wolfswinkel[1,2,3,4,5,*]
[1]Department of Molecular, Cellular, and Developmental Biology, Yale University, New Haven, CT 06511, USA
[2]Yale Stem Cell Center, Yale School of Medicine, New Haven, CT 06511, USA
[3]Center for RNA Biology and Medicine, Yale School of Medicine, New Haven, CT 06511, USA
[4]Center for Aging Research (Y-AGE), Yale School of Medicine, New Haven, CT 06511, USA
[5]Lead contact
*Correspondence: josien.van.wolfswinkel@yale.edu
https://doi.org/10.1016/j.cub.2026.02.050

SUMMARY

Most animals experience irreversibly declining health with advancing age, in part due to limitations in cell turnover and the accumulation of damage. The highly regenerative planarian *Schmidtea mediterranea* has abundant pluripotent stem cells that drive continuous cell turnover, yet it experiences an age-related loss of fertility, which can be restored through regeneration. We find that the source of planarian age-related infertility lies in the female reproductive system, accompanied by the formation of posterior ectopic ovaries and disrupted accessory reproductive structures, which are restored during regeneration. We further observe that the Notum/Wnt signaling gradient, which determines anterior-posterior polarity in planarians, is shifted posteriorly with age and that manipulating this gradient by RNAi was able to slow down or accelerate reproductive aging. These results indicate that in addition to a healthy stem cell pool, tissue polarity must be maintained to mitigate age-related decline and that resetting positional information could be a promising mechanism to promote tissue rejuvenation.

INTRODUCTION

Almost all animals experience a decline in organismal function over time that attenuates their maximum lifespan (MLS). This phenomenon, known as aging, is conserved across the animal kingdom. However, MLS itself is strikingly divergent, ranging from 3 days in the mayfly *Ephemera simulans*[1] to 507 years in the quahog *Arctica icelandica*.[2] For practical reasons, studies that investigate the mechanisms underlying aging have focused on short-lived model systems, such as *Caenorhabditis elegans* and *Mus musculus*, which have MLSs of around 30 days and 4 years, respectively.[3,4] Although many insights in the field of aging have resulted from the study of these organisms,[5,6] the short lifespans of common models may have precluded the discovery of degenerative processes that develop over longer timescales.

The freshwater planarian *Schmidtea mediterranea* represents a powerful model to study aging in long-lived animals. *S. mediterranea* is a tractable bilaterian that is used in the study of regeneration due to its remarkable ability to recover from almost any injury.[7,8] Its powerful regenerative capacity is conferred by a population of adult pluripotent stem cells ("neoblasts") that proliferate throughout the animal's entire lifespan.[9,10] The migration and differentiation of neoblasts are controlled by gradients of morphogens, such as Wnt family proteins, which direct the location and extent of organogenesis during homeostasis and regeneration.[11–13]

Although it can be propagated clonally through regeneration, the sexual S2 strain of *S. mediterranea* reproduces primarily through copulation. These hermaphroditic animals contain both male and female reproductive organs that are analogous to those in humans, including ovaries, testes, and accessory reproductive structures.[14–16] Zygotes result exclusively from cross-fertilization: partners exchange sperm during copulation, which fertilizes the oocytes of their partner.[15,17] Together with yolk cells produced by specialized glands, these zygotes are packaged into chitinous egg capsules, which are laid through the gonopore.[17,18] Embryogenesis occurs within the capsules until the hatchlings break out as newborn juveniles.

S. mediterranea has no known MLS and has been described as negligibly senescent.[19,20] This remarkable resilience to aging is believed to result from the neoblasts, which mediate constant homeostatic cell turnover, rejuvenating the animal by replacing age-damaged cells and organelles. Paradoxically, we and others observed that while the planarian lifespan is extremely long, its fertile period is rather brief but can be restored to youthful levels through regeneration.[21] If the neoblasts retain their functionality indefinitely, then why does fertility fail during aging, and how does regeneration promote its recovery?

Here, we provide evidence that the loss of fertility with age is due to the gradual disorganization of female reproductive structures, caused by drift of anterior-posterior (A-P) polarity. Regeneration resets this positional information, resulting in the restoration of functional female reproductive structures and recovery of youth-like fertility. Our findings reveal a surprising aspect to the maintenance of tissue health with age that is independent of the typical focus on cellular turnover during

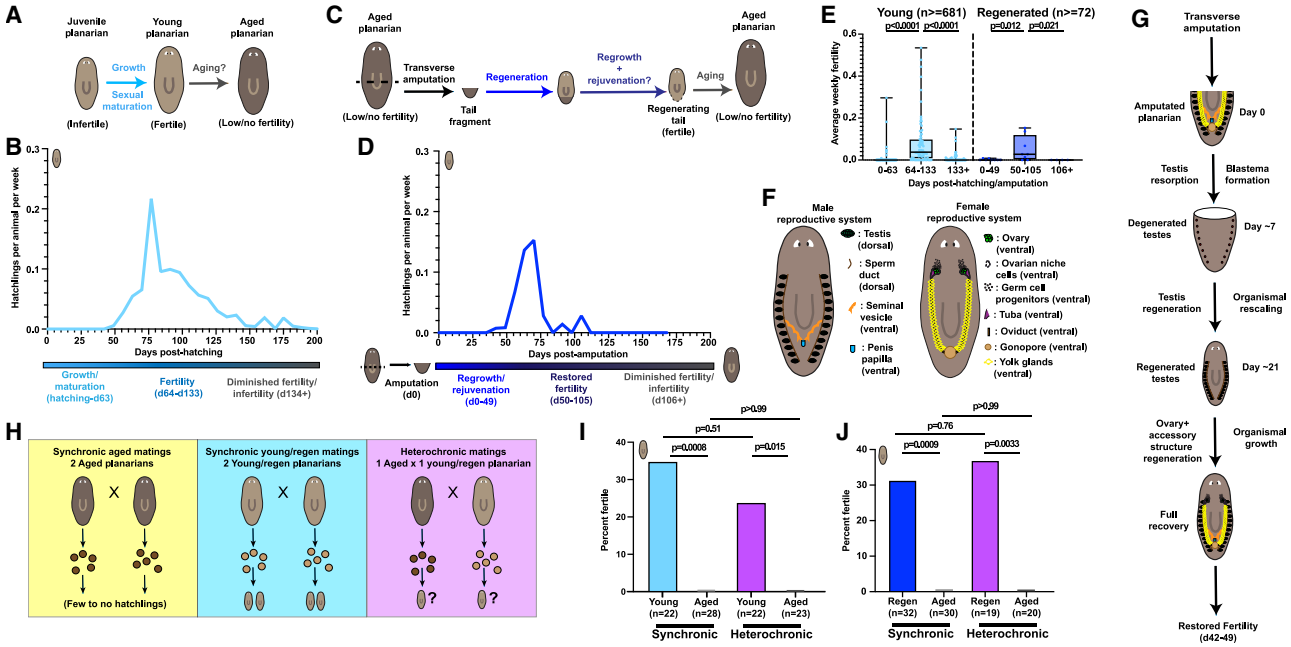

Figure 1. Aging planarians exhibit declining female fertility that is restored upon regeneration

(A) Schematic of fertility during the planarian lifecycle.

(B) Fertility curve showing average weekly offspring production in 8 cohorts of 27–136 planarians each (normalized per animal).

(C) Schematic of fertility during regeneration from transverse amputation.

(D) Fertility curve showing weekly hatchlings produced per animal in a cohort of 232 planarians.

(E) Weekly per animal hatchlings summarized into developmental segments representing growth/maturation, fertility, diminished fertility, regrowth/rejuvenation, restored fertility, and terminal diminished fertility. Error bars represent minimum and maximum observations. *p* values by Mann-Whitney U test.

(F) Schematic of planarian male (left) and female (right) reproductive systems.

(G) Schematic of germline regeneration. After head amputation, testes regress[22] and are recreated from germ cell progenitors (GCPs). In the new head, oocytes form from GCPs, restoring fertility by 42 dpa.[23]

(H) Schematic of the individual mating experiments. Single pairs of animals were separated after copulation, and their fertility was tracked in isolation.

(I and J) Percentage of animals from indicated crosses that exhibited fertility. Regenerated head fragments were used for (J). *p* values by Fisher's exact test.

See also Figure S1.

aging. Even in the presence of an ample supply of healthy stem cells to replace aging structures, the maintenance of tissue identity is here identified as a crucial regulatory process that needs to be upheld to sustain the physiology of long-lived organisms.

RESULTS

Planarian fertility decreases with age

We and others have observed that the fertility of *S. mediterranea* fluctuates over time.[21] To track changes in fertility over organismal age, we quantified the weekly offspring produced by cohorts of newly hatched animals for 200 days (Figure 1A). Newly hatched planarians lacked a developed germline, reaching sexual maturity after 6–9 weeks[17] (Figures 1B, 1E, S1A, S1D, and S1E). Fertility then rapidly peaked at 11 weeks post-hatching, before declining into near-complete infertility by 19 weeks. This decreased fertility could not be explained by organismal mortality, which did not occur during the first year of life (Figure S1B), nor by changes in capsule production. While capsule production declined with age (Figures S1D and S1E), phenotypically normal capsules with substantial yolk content were produced well beyond the end of the fertile window, affirming the notion that capsule production is necessary but not sufficient for fertility.[17,18] Our findings suggest that, contrary to previous assertions, sexually reproducing *Schmidtea mediterranea* are not entirely negligibly senescent, as they experience an age-associated decline in fertility. In fact, their fertile window is surprisingly brief given the organism's decades-long lifespan.

Regeneration restores fertility in aged planarians

Since regeneration mediates recovery from external damage, we wanted to test whether it could also repair internal dysfunctions such as the observed reproductive aging. Aged infertile planarians were amputated by parapharyngeal cross-section, and the offspring produced by both anterior (head) and posterior (tail) fragments was tracked for 175 days (Figures 1C and 1G). Remarkably, both tail and head fragments showed a significant restoration in fertility (Figures 1D, 1E, S1F, and S1G) and capsule production (Figures S1D, S1E, S1H, and S1I) lasting 7–8 weeks before returning to infertility. The length and level of fertility in tail fragments was comparable to young animals, suggesting that regeneration can partially reverse reproductive aging and restore fertility to youthful levels.

CellPress
OPEN ACCESS

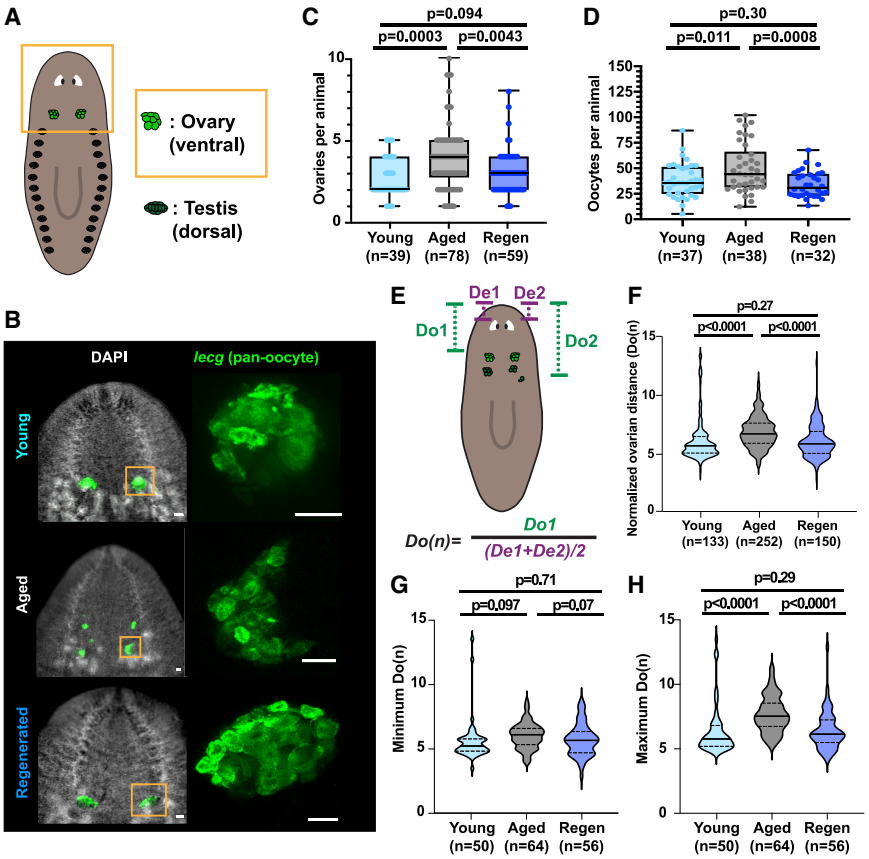

Figure 2. Aging planarians develop posterior ectopic ovaries

(A) Schematic showing the ovaries at the base of the head.

(B) (Left): representative widefield FISH images from young, aged, and regenerated animals showing oocytes (*lecg*) in green. (Right) Confocal projections of the boxed ovaries. Scale bar, 50 μm.

(C) Quantification of ovaries per animal. *p* values by Mann-Whitney U test.

(D) Quantification of oocytes per animal. *p* values by Welch's *t* test.

(E) Schematic showing how normalized ovarian distance (Do(n)) was computed.

(F–H) Quantification of overall (F), minimum (G, representing the anteriormost ovaries), and maximum (H, representing the posteriormost ovaries) Do(n) in aged, young, and regenerated animals. *p* values by Mann-Whitney U test.

Error bars on boxplots represent minimum and maximum observations. Solid lines in violin plots indicate medians, while dotted lines indicate quartile boundaries.

See also Figures S2 and S3.

Declining fertility originates from the female reproductive system

We next sought to identify the physiological causes of declining fertility with age. To determine whether infertility was caused by changes in the male or female germline (Figures 1F and 1G), we performed synchronic and heterochronic mating experiments (Figure 1H). Pairs of individual planarians were mated and then separated to track their offspring production in isolation. Since capsules laid by each planarian must have derived from that animal's own oocytes and their partner's sperm,[17,24] we were able to distinguish the paternal and maternal contributions to organismal fertility.

Consistent with our previous data, we found that synchronic pairs of aged planarians were completely infertile (Figures 1I and S1J), whereas synchronic pairs of young planarians showed significant fertility. In heterochronic pairs, aged planarians did not produce any offspring despite being provided sperm from a fertile partner, suggesting that aged planarians have an impairment in their female reproductive system. Conversely, the young members of those same pairings showed no significant reduction in fertility despite receiving sperm from an aged partner, indicating that aged planarians have no impairment in their male reproductive system and still transfer sperm during copulation. Similar results were obtained using regenerated animals instead of young animals (Figures 1J and S1K). We observed no significant differences in capsule production among any of the conditions (Figures S1L and S1M).

Declining fertility correlates with the appearance of ectopic ovaries

We next sought to uncover the physiological causes of age-related dysfunction in the female reproductive system. Planarian oocytes are produced by a pair of ovaries located at the base of the brain[15,16] (Figure 2A). To assay ovarian health, we performed fluorescent *in situ* hybridization (FISH) using the previously established oocyte marker *lecg*.[23] Surprisingly, while young animals contained a single pair of ovaries in the expected location, we found that aged animals formed ectopic ovarian structures, which were cleared by regeneration (Figures 2B, 2C, and S2A). To determine whether these ectopic ovaries resulted from fragmentation of existing ovaries or from *de novo* generation of new structures, we quantified the total number of oocytes per animal. We observed a significant increase in the number of oocytes per animal with age, suggesting that ectopic ovaries are newly created during aging (Figures 2D and S2B).

Previous studies suggested a link between ectopic ovaries in *S. mediterranea* and increased organismal size.[23] We found that while aged planarians tended to be larger, longer, and wider than their young or regenerated counterparts (Figures S3A and S3B), there was only a very weak correlation between these metrics of organismal size and the number of ovaries in aged animals, and no correlation at all in young or regenerated animals (Figures S3D, S3G, and S3J). To determine whether age was predictive of ectopic ovaries independent of animal size, we selected subpopulations of young, aged, and regenerated animals of similar surface area (Figure S3C), length (Figure S3F), or width (Figure S3I). Within these size-matched subpopulations, we consistently found that aged animals exhibited an increased number of ovaries compared with either young or regenerated counterparts (Figures S3E, S3H, and S3K). Taken together, our results indicate that while animal size may contribute to the

development of ectopic ovaries in aged animals, age alone is a significant predictor for the presence of ectopic ovaries.

Ectopic ovaries form in aberrant posterior locations

We noticed that the ectopic ovaries of aged animals formed pairs flanking the midline but were shifted in position along the A-P axis. To compare the A-P position of the aged ovaries with those of young and regenerated animals, we measured the distance between each ovary and the anterior tip of the animal, using eye position to control for variation in organismal size (Figure 2E). We found that ovaries in aged animals were located significantly more posterior to those in young or regenerated animals (Figure 2F). Further, we found that the minimum normalized ovarian distance (representing the anteriormost set of ovaries, Figure 2G) increased only slightly, while the maximum normalized ovarian distance (representing the posteriormost set of ovaries, Figure 2H) was greatly increased in aged animals. We observed similar trends when normalizing to brain length or width (Figures S2C and S2D), suggesting that aged ectopic ovaries form posterior to the original pair.

Ovarian attributes are unevenly divided between anterior and posterior ovaries

To understand why fertility declined in aged planarians despite an increased number of ovaries, we investigated the oocytes, their progenitors, and associated accessory reproductive structures. It was previously reported that ovaries contain both early and late oocytes, classified based upon cell size, position, and shape[23] (Figure 3A). We observed that young and regenerated ovaries contained both oocyte stages, but that a significant percentage of aged ovaries lacked the smaller early oocytes (Figures 3B and 3C). This effect was significantly stronger in the posterior ovaries of aged animals compared with anterior ovaries or ovaries that resided alone in their flank (Figures 3D–3F). Early oocytes derive from a population of germ cell progenitors (GCPs) that localize as a proximal population around each ovary and a "spray" of cells in the anterior direction[23,25] (Figure 3A). Using FISH for the germ cell marker *nanos*,[23] we found that aged planarians exhibited a significant depletion of GCPs compared with young and regenerated counterparts (Figures 3G–3J, Figures S4A–S4C). Within aged animals, the anterior ovaries had slightly higher numbers of GCPs than posterior ovaries, and single ovaries had significantly higher numbers of GCPs than both (Figures 3K, 3L, S4, and S4D). These results suggest that primarily the posterior ovaries of aged *S. mediterranea* experience GCP depletion, which restricts the supply of early oocytes and could cause accumulation of damaged or dysfunctional late oocytes.

We next assayed the physiology of accessory reproductive structures, including the ovarian niche cells surrounding the ovary and the tubas and oviducts connected at the posterior end. Using FISH for the niche marker *ece-1*,[23] we found that ovaries of all ages were similarly supported by niche cells (Figures S4E–S4H). The organization of the tuba and oviducts, however, was markedly different in aged animals. FISH for the oviduct and tubal marker *nhr-1*[26] (Figure 4A) showed that in young and regenerated animals, the posterior end of each ovary was associated with a funnel-shaped tuba (Figure 4B) that transitioned into the oviduct. In aged animals, these structures were frequently disconnected from the ovaries they served (Figure 4C). To address the effect of ovarian position, we again focused on aged animals, finding that almost 50% of anterior ovaries lacked proper connections to the oviducts and/or tubas, while both single and posterior ovaries showed low levels of disconnection (Figures 4D and 4E). Given that the tuba and oviducts are essential for fertilization, aged anterior ovaries that are not connected likely cannot contribute to the generation of offspring.

Taken together, these results indicate that the formation of ectopic ovaries results in a physical separation between the types of cells recruited by each ovary: anterior ovaries recruit the majority of GCPs to form new oocytes, while posterior ovaries are connected to the oviducts and tubas. This results in two separate structures, neither of which is capable of executing the complete suite of essential ovarian functions, which may explain the decreased fertility of aged planarians.

Anterior tissue identity is extended with age and is reset by regeneration

Planarian organogenesis is regulated by morphogen gradients along the body axes.[11,12] For example, the morphogen Wnt is enriched in the posterior of the animal, while the Wnt antagonist Notum is primarily produced in the anterior pole, creating a gradient of Wnt activity along the A-P axis that regulates neoblasts.[11,13,27] Since altered expression of Wnt proteins can cause ectopic organogenesis along the A-P axis,[10–13,28,29] we sought to determine whether similar changes underly the formation of ectopic ovaries during aging.

Using FISH to identify *notum*-expressing cells (Figure 5A), we found that aged animals had a significantly greater number of *notum*+ anterior pole cells spread over a greater area (Figures 5B, 5C, S5A, and S5B) but at similar density (Figures S5C) compared with young or regenerated animals, likely increasing the spatial reach of Notum signaling. To determine whether this was counterbalanced by changes in Wnt levels, we performed FISH against the posterior pole marker *wnt1* (Figure S5D).[11] We found that levels of *wnt1* did not significantly increase with age (Figures S5E–S5G) even though the normalized distance between the ovaries and the posterior pole was significantly increased (Figure S4E and S4H). Taken together, these results support a model wherein with age, levels of Notum increase in the anterior tip, while the number of *wnt1*+ cells remains constant, and those cells become more distant. On net, this induces an expansion in anterior identity that may explain the formation of posterior ectopic ovaries with age (Figure 5D).

Modulating Wnt signaling recapitulates features of reproductive aging

To test whether these changes in A-P polarity could be responsible for age-related defects in germline organization and fertility, we performed RNAi-mediated knockdowns of the Wnt inhibitor *notum* and the Wnt transducer *beta-catenin* in cohorts of fertile regenerated animals (Figure 6A). As anterior identity expands with age, we hypothesized that preventing this expansion through *notum* RNAi would slow reproductive aging while *beta-catenin* RNAi would hasten it. Our results were consistent with this hypothesis: *notum* RNAi-treated animals showed increased fertility (Figures 6B, 6C, S6A, S6B, S6D, and S6E)

CellPress
OPEN ACCESS

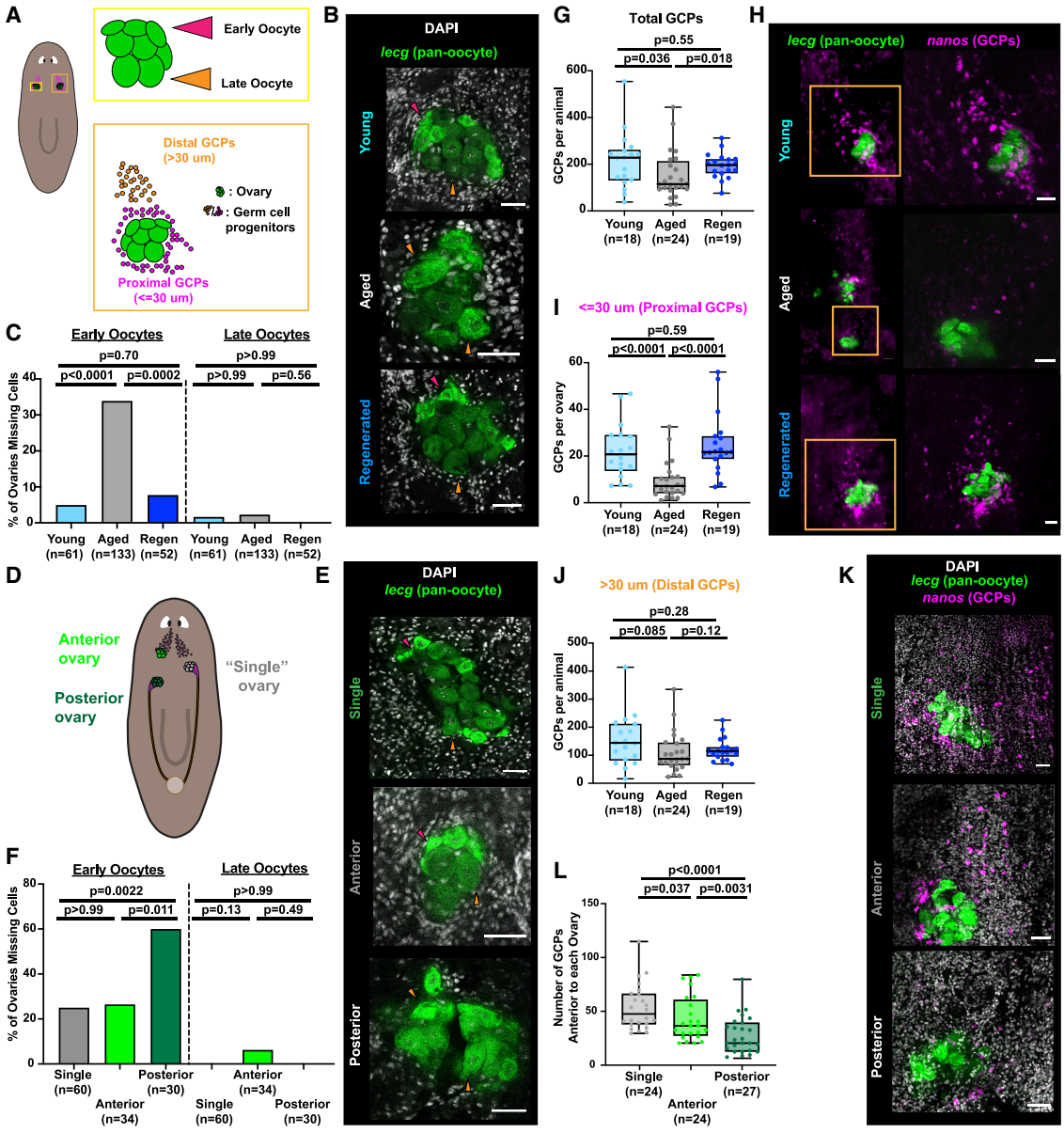

Figure 3. Aging planarians have depleted germ cell and early oocyte pools in posterior ovaries

(A) Schematic showing early and late oocytes within the ovary, as well as the GCP populations that produce them.[23]

(B) Representative confocal slices of ovaries in aged, young, and regenerated animals. Indicated are early oocytes (magenta arrowheads) and late oocytes (orange arrowheads). Scale bar, 50 μm.

(C) Percentage of ovaries that lack early (left) or late (right) oocytes. *p* values by Fisher's exact test.

(D) Schematic showing single, anterior, and posterior ovaries in aged planarians.

(E) Representative confocal slices showing the presence of early (magenta arrowhead) and late (orange arrowhead) *lecg*+ oocytes in single, anterior, and posterior ovaries in aged planarians. Scale bar, 50 μm.

(F) Percentage of ovaries lacking early (left), or late (right) oocytes in aged planarians. *p* values by Fisher's exact test.

(G) Quantification of total GCPs per animal. *p* values by Mann-Whitney U test.

(H) Left: Representative widefield FISH images, showing pan-oocyte marker *lecg* and GCP marker *nanos*. Right: Confocal projections. Scale bar, 50 μm.

(I and J) Quantification of proximal GCPs per ovary (I), or distal GCPs per animal (J). *p* values by Mann-Whitney U test.

(K) Representative confocal projections of the distribution of *nanos*+ GCPs over single, anterior, and posterior *lecg*+ ovaries in aged planarians. Scale bar, 50 μm.

(L) Quantification of GCPs anterior to single, anterior, and posterior ovaries in aged animals. *p* values by Mann-Whitney U test.

Error bars represent minimum and maximum observations.

See also Figure S4.

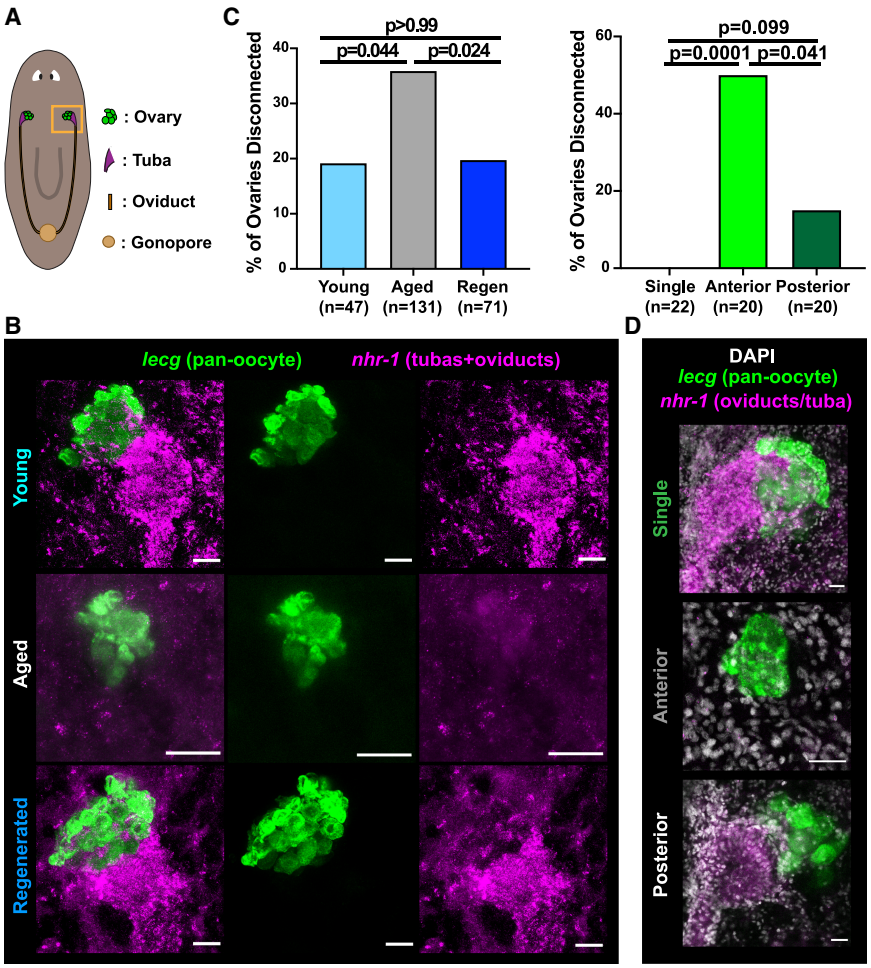

Figure 4. Aging planarians lack oviduct/tuba connections in anterior ovaries

(A) Schematic showing the oviducts and tubas connected to the ovaries.

(B) Representative confocal projections of FISH samples in aged, young, and regenerated animals, showing the pan-oocyte marker *lecg* and the oviduct/tuba marker *nhr-1*. Scale bar, 50 μm.

(C) Percentages of aged, young, and regenerated ovaries lacking proper connections to oviducts/tubas. *p* values by Fisher's exact test.

(D) Representative confocal projections showing the connection of anterior, posterior, and single ovaries (*lecg*) to the oviducts/tubas (*nhr-1*) in aged planarians. Scale bar, 25 μm.

(E) Percentages of anterior, posterior, and single ovaries lacking proper connections to the tubas/oviducts in aged planarians. *p* values by Fisher's exact test.

and extended fertile period (Figures 6D, S6C, and S6F), whereas *beta-catenin* RNAi animals were completely sterile. These results indicate that restricting anterior identity is sufficient to extend fertility in *S. mediterranea* and that expanding anterior identity induces infertility.

Curiously, 64% of *beta-catenin* RNAi animals contained up to 12 posterior ectopic ovaries, while 24% exhibited complete ovarian degeneration (Figures 6E, 6F, and S7A–S7C). By contrast, none of the control animals had fewer than two ovaries. Among animals that possessed ectopic ovaries, the *beta-catenin* RNAi animals contained significantly more ovaries compared with age-matched controls (Figures 6G, S7D, and S7E). Furthermore, *beta-catenin* RNAi animals had a significant increase in normalized ovarian distance due to their numerous but small posterior ectopic ovaries (Figures 6H–6K and S7F). Additionally, the GCP population was reduced in *beta-catenin* RNAi animals (Figures 6L–6N), and the remaining GCPs were strongly depleted from the region anterior to the ovaries, instead residing around the posterior ectopic ovaries (Figures 6M, 6O, 6P, S7G, and S7H), consistent with an expansion in anterior identity due to loss of Wnt signaling. Finally, both anterior and posterior ovaries in *beta-catenin* RNAi animals lacked associated tubal structures (Figures 6Q–6S). Taken together, these results demonstrate that *beta-catenin* RNAi animals recapitulate many age-related planarian reproductive phenotypes at an accelerated rate, including loss of fertility, formation of posterior ectopic ovaries, GCP depletion, and ovarian disconnection.

We also sought to determine if *notum* RNAi animals experienced delayed development of age-related pathologies concomitant with their improved fertility. We found that *notum* RNAi animals exhibited more youthful reproductive physiology: while *notum* RNAi animals still formed posterior ectopic ovaries (Figures S7I–S7O), they had a significant expansion in their GCP pool (Figures 6T–6V and S7P–S7R) concentrated above single and posterior ovaries (Figures 6W, S7S, and S7T) and a slight increase in the connectivity of posterior ovaries to the oviducts and tubas (Figures S7U–S7W). These results can explain why *notum* RNAi animals recover fertility while forming ectopic ovaries: increased overall levels of GCPs allow a greater number of cells to "escape" capture by the anterior ovaries and migrate down to feed the posterior ovaries. Thus, instead of possessing two partially functional sets of ovaries, the posterior ovaries in *notum* RNAi animals may retain full functionality due to an elevated level of associated GCPs.

Taken together, these results demonstrate that Wnt signaling and controlled production of Notum play a crucial role in regulating female fertility and reproductive physiology and that altering Wnt signaling using RNAi can accelerate or slow down the development of pathologies associated with reproductive aging.

DISCUSSION

Long-lived organisms present a valuable opportunity to study age-related phenotypes that are masked by organismal mortality in short-lived animals, as well as novel mechanisms to resist aging. Here, we used the planarian *S. mediterranea*, which has an indefinite lifespan,[19,20] to reveal age-related changes in germline function. We discovered that maintenance of positional identity

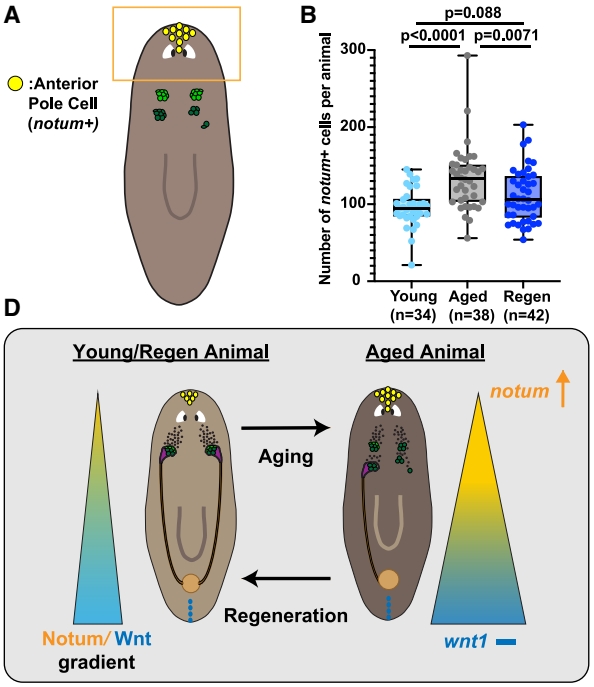

Figure 5. Anterior-posterior positioning information is disrupted in aged planarians and reset by regeneration

(A) Schematic showing the *notum*+ anterior pole cells.

(B) Quantification of *notum*+ cells per animal. *p* values by Mann-Whitney U test. Error bars represent minimum and maximum observations.

(C) Representative confocal projections of FISH samples, showing *notum* (magenta) in the anterior tips. Scale bar, 50 μm.

(D) Model hypothesizing how positional information derived from localized *notum* expression may explain the formation of ectopic ovaries in planarians with age.

See also Figure S5.

is a major challenge for *S. mediterranea* and that deregulation of positional cues with age promotes the loss of fertility in this long-lived system.

While *S. mediterranea* is considered negligibly senescent,[19,20] we find that these animals develop age-related ovarian pathologies including a declining GCP population as well as a gradual deregulation of germline composition and structure. Organization of planarian tissue is dictated by a set of morphogens that ensure that stem cells generate position-appropriate structures. The main morphogen regulating A-P identity is Wnt, which is produced in the posterior tip of the animal and is counteracted by the Wnt inhibitor Notum in the anterior.[11–13,29–31] We find that as *S. mediterranea* ages, levels of *notum* in the anterior tip of the animal increase, shifting the A-P gradient in the posterior direction and creating posterior ectopic ovaries. The formation of these ectopic structures splits the function of the ovaries across the A-P axis: the anterior ovaries interact with cues from above, capturing the majority of GCPs, while the posterior ovaries interface with the oviducts and tubas from below. Ultimately, this creates a pair of ovaries with separated attributes that cannot sustain full functionality.

Our results indicate that age-related changes in positional control genes contribute to declining fertility. Increasing Wnt signaling by knockdown of *notum* prolonged reproductive lifespan, while impairing Wnt signaling by knockdown of *beta-catenin* attenuated it. Additionally, *notum* RNAi recapitulated key features of reproductive youthfulness, such as increased GCP number, while *beta-catenin* RNAi animals experienced signs of premature ovarian dysfunction, including GCP depletion and formation of posterior ectopic ovaries. While these treatments do not recapitulate every phenotype of reproductive aging in *S. mediterranea*, they demonstrate that maintenance of organismal polarity through the Wnt/Notum signaling gradient is essential for female reproductive structure and function.

Although we show that Wnt/Notum signaling regulates ovarian physiology and function, this regulation may occur indirectly through tissues such as the brain, which controls the reproductive system through neuropeptides including NPY-8.[32,33] We have found that RNAi against Wnt genes expressed in the brain such as *wnt5*[34] and *wntA*[12] can alter ovarian count and positioning (Figure S7X). Further, previous studies have found that the relative size of the brain and its neuronal composition are subtly altered with age.[21] Future study of the brain-ovary signaling axes will improve our understanding of these potential interactions.

Regardless of the mechanism, it is remarkable that inability to maintain positional identity can drive reproductive aging. *S. mediterranea*'s unique ability to rebuild position-restricted organs *de novo* allowed us to discover this hitherto-unappreciated relationship between positional information and aging. This relationship is however not unprecedented: declining Wnt signaling with age occurs in vertebrate organ systems,[35–37] including ovaries,[38,39] suggesting that Wnt dysregulation may be a conserved contributor to female reproductive aging. Whether these other cases of decreased Wnt signaling with age also involve alterations in spatial organization remains to be investigated.

It may seem paradoxical that *S. mediterranea* has a short reproductive period despite its extremely long lifespan. However, age-related infertility in planarians is not a permanent state: upon injury, Wnt and Notum are transiently upregulated at the wound site before respecification of a new anterior or posterior pole,[11,13] which resets the animal to a more youthful Wnt/Notum gradient and may restore organismal physiology and fertility. Periodic regeneration may thus be an essential part of the planarian lifecycle. Interestingly, our data show that, even when kept under optimal conditions, 30%–40% of animals experienced injury during their first year of life (Figure S1C). In the wild, where dangers are more abundant, injury and regeneration may occur more frequently, resulting in a natural periodic reset of positional information and fertility.

Interestingly, resilience to aging is coupled with regenerative abilities in many organisms. Within flatworms, species that have robust regeneration, such as *Schmidtea polychroa*, *Girardia*

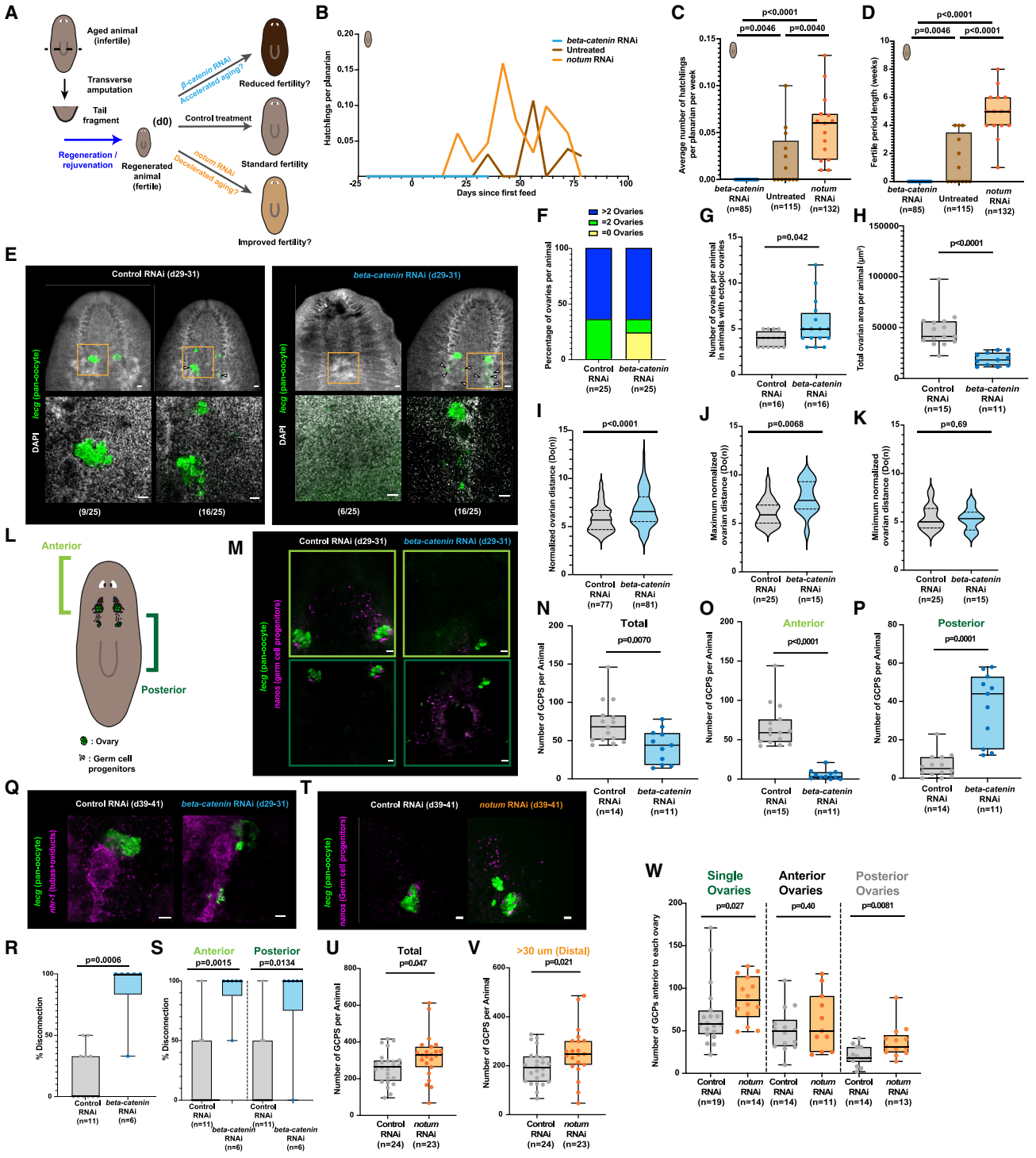

Figure 6. Altering anterior-posterior identity by targeting *notum* and *beta-catenin* modulates reproductive aging

(A) Schematic of RNAi experiments. RNAi started 57–65 dpa. Fertility was tracked for the next 11 weeks; female reproductive physiology was assayed at 39–41 days of RNAi. *Beta-catenin* RNAi animals were assayed at 29–31 days due to developing polarity defects.

(B) Fertility curve showing weekly hatchlings per animal (13–15 cohorts of 6–10 planarians each per treatment).

(C) Average number of weekly hatchlings per animal across cohorts. *p* values by Mann-Whitney U test.

(D) Quantification of the time between laying of first and last hatchling. *p* values by Mann-Whitney U test.

(E) (Top): Representative widefield FISH images of ovaries (*lecg*, green) in control (left), and *beta-catenin* RNAi (right) animals. White arrowheads indicate posterior ectopic ovaries. (Bottom) Confocal projections of boxed ovaries. Scale bar, 50 μm.

(F) Binned quantification of ovarian phenotypes.

(legend continued on next page)

tigrina, and the more distantly related turbellarian *Stenostomum leucops*,[40–42] have long lifespans,[20,43–45] whereas *Macrostomum lignano*, a turbellarian with limited regenerative capacity,[46,47] exhibits a mortality rate similar to that of rodents.[48] This correlation between regeneration and agelessness extends beyond planarians: many long-lived organisms such as *Hydra vulgaris* exhibit profound regenerative capacity,[49] and preliminary data from Haluza et al. indicate that regeneration reduces epigenetic age in *Ambystoma mexicanum*.[50] In combination with these findings, our results suggest that the use of regeneration to promote rejuvenation may be a widespread phenomenon.

While the phenotypes observed in this study focus on the germline, it is possible that other planarian tissues also become disorganized with age and that regeneration serves as a global rejuvenation strategy. A recent study described several age-related changes in planarian tissues,[21] many of which involve alterations in spatial organization, such as the formation of ectopic eyes. These phenomena may similarly be dependent on the regeneration-mediated resetting of positional identity described in this study. Furthermore, in some planarians, genes that counteract hallmarks of aging are induced upon regeneration, such as telomerase in *S. mediterranea*[51] or *atg8* in *Dugesia japonica*.[52,53] Further experiments are needed to determine whether regeneration promotes clearance of other age-related biomarkers in *S. mediterranea*.

Taken together, our results demonstrate that *S. mediterranea*, despite its extreme longevity, experiences a hitherto-undercharacterized form of age-related germline dysfunction driven by loss of organismal polarity, which can be cleared through regeneration-coupled rejuvenation. These exciting results highlight the relationship between maintenance of positional information and longevity, which merits further study in planarians and beyond.

RESOURCE AVAILABILITY

Lead contact

Requests for further information and resources should be directed to and will be fulfilled by the lead contact, Dr. Josien C. van Wolfswinkel (josien.van.wolfswinkel@yale.edu).

Materials availability

All unique and stable reagents generated in this study are available from the lead contact without restriction.

Data and code availability

- Microscopy data reported in this paper will be shared by the lead contact upon request.
- This paper does not report original code. Some images contained in this study were analyzed using the planarian image quantification program (PIQ),[54] which can be found at GitLab: https://gitlab.com/vanwolfswinkel/PIQ. Configuration files used in the analysis are described in Data S1.
- Any additional information required to reanalyze the data reported in this paper is available from the lead contact upon request.

ACKNOWLEDGMENTS

We thank the members of the van Wolfswinkel lab for their input and discussion. We acknowledge the Yale Science Hill Imaging Facility for access to the confocal microscope, as well as for training and technical support. This research was supported by NIH grants R01AG078926 (PI: J.C.v.W.) and F31AG081110 (PI: Andrew Verdesca), as well as by the Vallee Foundation (PI: J.C.v.W.).

AUTHOR CONTRIBUTIONS

Conceptualization, A.V. and J.C.v.W.; investigation, A.V. and M.B.; methodology, A.V. and J.C.v.W.; software, A.P. and J.C.v.W.; supervision, J.C.v.W.; visualization, A.V., A.P., and J.C.v.W.; writing (original draft), A.V. and J.C.v.W.; writing (review and editing), A.V., A.P., M.B., and J.C.v.W.

DECLARATION OF INTERESTS

The authors declare no competing interests.

STAR★METHODS

Detailed methods are provided in the online version of this paper and include the following:

- KEY RESOURCES TABLE
- EXPERIMENTAL MODEL AND STUDY PARTICIPANT DETAILS
  - Planarian culture and husbandry
- METHOD DETAILS
  - Heterochronic and synchronic mating experiments

(G) Quantification of ovaries per animal in specimens that possess at least one ectopic ovary in control and *beta-catenin* RNAi animals. *p* values by Mann-Whitney U test.
(H) Quantification of the total area of oocyte (*lecg*) signal per animal in control and *beta-catenin* RNAi animals. *p* values by Welch's *t* test.
(I–K) Quantification of the overall (I), maximum (J), and minimum (K) normalized ovarian distance in control and *beta-catenin* RNAi animals. *p* values by Welch's *t* test.
(L) Schematic of ovaries and GCPs in control and *beta-catenin* RNAi animals.
(M) Representative widefield images of the anterior (top) and posterior (bottom) regions of control (left) and *beta-catenin* RNAi (right) animals showing oocytes (*lecg*, green) and GCPs (*nanos*, magenta). Overlap between the top and bottom images shows their anatomical relationship. Scale bar=50 μm.
(N–P) Quantification of the total (N), anterior (O), and posterior (P) GCPs in control and *beta-catenin* RNAi animals. *p* values by Welch's *t* test.
(Q) Representative confocal projections showing ovaries (*lecg*, green) and the oviduct/tuba (*nhr-1*, magenta) in control and *beta-catenin* RNAi animals. Scale bar, 50 μm.
(R) Percentage of ovaries per animal lacking proper connections to oviducts/tubas. *p* values by Mann-Whitney U test.
(S) Percentages of anterior (left) and posterior (right) ovaries per animal lacking proper connections to tubas/oviducts in control and *beta-catenin* RNAi animals. *p* values by Mann-Whitney U test.
(T) Representative confocal projections showing oocytes (*lecg*, green) and GCPs (*nanos*, magenta) in control (left) and *notum* RNAi animals (right). Scale bar, 50 μm.
(U and V) Quantification of the total (U) and distal (V) GCPs per animal in control and *notum* RNAi animals. *p* values by Welch's *t* test.
(W) Quantification of GCPs anterior to single (left), anterior (center), and posterior (right) ovaries in control and *notum* RNAi animals. *p* values by Welch's *t* test for anterior ovaries, and by Mann-Whitney U test for single and posterior ovaries.
Error bars of boxplots represent minimum and maximum observations. Solid lines on violin plots indicate medians, while dotted lines indicate quartile boundaries. See also Figures S6–S7.

- RNA interference
- Fluorescent in situ hybridization
- Image scoring and quantification

- QUANTIFICATION AND STATISTICAL ANALYSIS

SUPPLEMENTAL INFORMATION

Supplemental information can be found online at https://doi.org/10.1016/j.cub.2026.02.050.

Received: September 29, 2025
Revised: January 5, 2026
Accepted: February 24, 2026
Published: March 23, 2026

REFERENCES

1. Carey, J.R. (2002). Longevity minimalists: life table studies of two species of northern Michigan adult mayflies. Exp. Gerontol. *37*, 567–570. https://doi.org/10.1016/S0531-5565(01)00180-2.
2. Butler, P.G., Wanamaker, A.D., Scourse, J.D., Richardson, C.A., and Reynolds, D.J. (2013). Variability of marine climate on the North Icelandic Shelf in a 1357-year proxy archive based on growth increments in the bivalve Arctica islandica. Palaeogeogr. Palaeoclimatol. Palaeoecol. *373*, 141–151. https://doi.org/10.1016/j.palaeo.2012.01.016.
3. Kenyon, C., Chang, J., Gensch, E., Rudner, A., and Tabtiang, R. (1993). A C. elegans mutant that lives twice as long as wild type. Nature *366*, 461–464. https://doi.org/10.1038/366461a0.
4. Austad, S.N. (1997). Comparative aging and life histories in mammals. Exp. Gerontol. *32*, 23–38. https://doi.org/10.1016/S0531-5565(96)00059-9.
5. López-Otín, C., Blasco, M.A., Partridge, L., Serrano, M., and Kroemer, G. (2013). The hallmarks of aging. Cell *153*, 1194–1217. https://doi.org/10.1016/j.cell.2013.05.039.
6. López-Otín, C., Blasco, M.A., Partridge, L., Serrano, M., and Kroemer, G. (2023). Hallmarks of aging: An expanding universe. Cell *186*, 243–278. https://doi.org/10.1016/j.cell.2022.11.001.
7. Newmark, P.A., and Sánchez Alvarado, A. (2002). Not your father's planarian: a classic model enters the era of functional genomics. Nat. Rev. Genet. *3*, 210–219. https://doi.org/10.1038/nrg759.
8. Morgan, T.H. (1898). Experimental Studies of the Regeneration of Planaria maculata. Arch. Entwickelungsmechanik Org. *7*, 364–397. https://doi.org/10.1007/BF02161491.
9. Newmark, P.A., and Sánchez Alvarado, A. (2000). Bromodeoxyuridine Specifically Labels the Regenerative Stem Cells of Planarians. Dev. Biol. *220*, 142–153. https://doi.org/10.1006/dbio.2000.9645.
10. van Wolfswinkel, J.C., Wagner, D.E., and Reddien, P.W. (2014). Single-cell analysis reveals functionally distinct classes within the planarian stem cell compartment. Cell Stem Cell *15*, 326–339. https://doi.org/10.1016/j.stem.2014.06.007.
11. Petersen, C.P., and Reddien, P.W. (2009). A wound-induced Wnt expression program controls planarian regeneration polarity. Proc. Natl. Acad. Sci. USA *106*, 17061–17066. https://doi.org/10.1073/pnas.0906823106.
12. Hill, E.M., and Petersen, C.P. (2015). Wnt/Notum spatial feedback inhibition controls neoblast differentiation to regulate reversible growth of the planarian brain. Development *142*, 4217–4229. https://doi.org/10.1242/dev.123612.
13. Petersen, C.P., and Reddien, P.W. (2011). Polarized notum activation at wounds inhibits Wnt function to promote planarian head regeneration. Science *332*, 852–855. https://doi.org/10.1126/science.1202143.
14. Issigonis, M., and Newmark, P.A. (2019). From worm to germ: Germ cell development and regeneration in planarians. Chapter Four. In Current Topics in Developmental Biology, R. Lehmann, ed. (Academic Press), pp. 127–153. https://doi.org/10.1016/bs.ctdb.2019.04.001.
15. Stevens, N.M. (1904). On the Germ Cells and the Embryology of Planaria simplissima. In Proceedings of the National Academies of Science, pp. 208–229.
16. Chong, T., Stary, J.M., Wang, Y., and Newmark, P.A. (2011). Molecular markers to characterize the hermaphroditic reproductive system of the planarian Schmidtea mediterranea. BMC Dev. Biol. *11*, 69. https://doi.org/10.1186/1471-213X-11-69.
17. Guo, L., Zhang, S., Rubinstein, B., Ross, E., and Alvarado, A.S. (2016). Widespread maintenance of genome heterozygosity in Schmidtea mediterranea. Nat. Ecol. Evol. *1*, 19. https://doi.org/10.1038/s41559-016-0019.
18. Steiner, J.K., Tasaki, J., and Rouhana, L. (2016). Germline Defects Caused by Smed-boule RNA-Interference Reveal That Egg Capsule Deposition Occurs Independently of Fertilization, Ovulation, Mating, or the Presence of Gametes in Planarian Flatworms. PLOS Genet. *12*, e1006030. https://doi.org/10.1371/journal.pgen.1006030.
19. Sahu, S., Dattani, A., and Aboobaker, A.A. (2017). Secrets from immortal worms: What can we learn about biological ageing from the planarian model system? Semin. Cell Dev. Biol. *70*, 108–121. https://doi.org/10.1016/j.semcdb.2017.08.028.
20. Mouton, S., Willems, M., Houthoofd, W., Bert, W., and Braeckman, B.P. (2011). Lack of metabolic ageing in the long-lived flatworm Schmidtea polychroa. Exp. Gerontol. *46*, 755–761. https://doi.org/10.1016/j.exger.2011.04.003.
21. Dai, X., Li, X., Tyshkovskiy, A., Zuckerman, C., Cheng, N., Lin, P., Paris, D., Qureshi, S., Kruglyak, L., Mao, X., et al. (2025). Regeneration leads to global tissue rejuvenation in aging sexual planarians. Nat. Aging *5*, 780–798. https://doi.org/10.1038/s43587-025-00847-9.
22. Wang, Y., Zayas, R.M., Guo, T., and Newmark, P.A. (2007). nanos function is essential for development and regeneration of planarian germ cells. Proc. Natl. Acad. Sci. USA *104*, 5901–5906. https://doi.org/10.1073/pnas.0609708104.
23. Khan, U.W., and Newmark, P.A. (2022). Somatic regulation of female germ cell regeneration and development in planarians. Cell Rep. *38*, 110525. https://doi.org/10.1016/j.celrep.2022.110525.
24. Davies, E.L., Lei, K., Seidel, C.W., Kroesen, A.E., McKinney, S.A., Guo, L., Robb, S.M.C., Ross, E.J., Gotting, K., and Alvarado, A.S. (2017). Embryonic origin of adult stem cells required for tissue homeostasis and regeneration. eLife *6*, e21052. https://doi.org/10.7554/eLife.21052.
25. Handberg-Thorsager, M., and Saló, E. (2007). The planarian nanos-like gene Smednos is expressed in germline and eye precursor cells during development and regeneration. Dev. Genes Evol. *217*, 403–411. https://doi.org/10.1007/s00427-007-0146-3.
26. Tharp, M.E., Collins, J.J., 3rd, and Newmark, P.A. (2014). A lophotrochozoan-specific nuclear hormone receptor is required for reproductive system development in the planarian. Dev. Biol. *396*, 150–157. https://doi.org/10.1016/j.ydbio.2014.09.024.
27. Kakugawa, S., Langton, P.F., Zebisch, M., Howell, S.A., Chang, T.-H., Liu, Y., Feizi, T., Bineva, G., O'Reilly, N., Snijders, A.P., et al. (2015). Notum deacylates Wnt proteins to suppress signalling activity. Nature *519*, 187–192. https://doi.org/10.1038/nature14259.
28. Cebrià, F., Kobayashi, C., Umesono, Y., Nakazawa, M., Mineta, K., Ikeo, K., Gojobori, T., Itoh, M., Taira, M., Sánchez Alvarado, A.S., et al. (2002). FGFR-related gene nou-darake restricts brain tissues to the head region of planarians. Nature *419*, 620–624. https://doi.org/10.1038/nature01042.
29. Hill, E.M., and Petersen, C.P. (2018). Positional information specifies the site of organ regeneration and not tissue maintenance in planarians. eLife *7*, e33680. https://doi.org/10.7554/eLife.33680.
30. Chong, T., Collins, J.J., 3rd, Brubacher, J.L., Zarkower, D., and Newmark, P.A. (2013). A sex-specific transcription factor controls male identity in a simultaneous hermaphrodite. Nat. Commun. *4*, 1814. https://doi.org/10.1038/ncomms2811.
31. Stückemann, T., Cleland, J.P., Werner, S., Thi-Kim Vu, H., Bayersdorf, R., Liu, S.Y., Friedrich, B., Jülicher, F., and Rink, J.C. (2017). Antagonistic Self-Organizing Patterning Systems Control Maintenance and

Regeneration of the Anteroposterior Axis in Planarians. Dev. Cell *40*, 248–263.e4. https://doi.org/10.1016/j.devcel.2016.12.024.

32. Collins, J.J., 3rd, Hou, X., Romanova, E.V., Lambrus, B.G., Miller, C.M., Saberi, A., Sweedler, J.V., and Newmark, P.A. (2010). Genome-wide analyses reveal a role for peptide hormones in planarian germline development. PLOS Biol. *8*, e1000509. https://doi.org/10.1371/journal.pbio.1000509.
33. Rouhana, L., Tasaki, J., Saberi, A., and Newmark, P.A. (2017). Genetic dissection of the planarian reproductive system through characterization of Schmidtea mediterranea CPEB homologs. Dev. Biol. *426*, 43–55. https://doi.org/10.1016/j.ydbio.2017.04.008.
34. Adell, T., Salò, E., Boutros, M., and Bartscherer, K. (2009). Smed-Evi/Wntless is required for β-catenin-dependent and-independent processes during planarian regeneration. Development *136*, 905–910. https://doi.org/10.1242/dev.033761.
35. Hofmann, J.W., McBryan, T., Adams, P.D., and Sedivy, J.M. (2014). The effects of aging on the expression of Wnt pathway genes in mouse tissues. Age (Dordr) *36*, 9618. https://doi.org/10.1007/s11357-014-9618-3.
36. Ogamino, S., Yamamichi, M., Sato, K., and Ishitani, T. (2024). Dynamics of Wnt/β-catenin reporter activity throughout whole life in a naturally short-lived vertebrate. NPJ Aging *10*, 23. https://doi.org/10.1038/s41514-024-00149-1.
37. Rauner, M., Sipos, W., and Pietschmann, P. (2008). Age-dependent Wnt gene expression in bone and during the course of osteoblast differentiation. Age (Dordr) *30*, 273–282. https://doi.org/10.1007/s11357-008-9069-9.
38. Xu, D., Song, S., Wang, F., Li, Y., Li, Z., Yao, H., Zhao, Y., and Zhao, Z. (2023). Single-cell transcriptomic atlas of goat ovarian aging. J. Anim. Sci. Biotechnol. *14*, 151. https://doi.org/10.1186/s40104-023-00948-8.
39. Ren, W., Wang, J., Zeng, Y., Wang, T., Meng, J., and Yao, X. (2024). Differential age-related transcriptomic analysis of ovarian granulosa cells in Kazakh horses. Front. Endocrinol. (Lausanne) *15*, 1346260. https://doi.org/10.3389/fendo.2024.1346260.
40. Vila-Farré, M., Rozanski, A., Ivanković, M., Cleland, J., Brand, J.N., Sandberg, F., Grohme, M.A., von Kannen, S., Grosbusch, A.L., Vu, H.T.K., et al. (2023). Evolutionary dynamics of whole-body regeneration across planarian flatworms. Nat. Ecol. Evol. *7*, 2108–2124. https://doi.org/10.1038/s41559-023-02221-7.
41. Cebrià, F., Vispo, M., Newmark, P., Bueno, D., and Romero, R. (1997). Myocyte differentiation and body wall muscle regeneration in the planarian Girardia tigrina. Dev. Genes Evol. *207*, 306–316. https://doi.org/10.1007/s004270050118.
42. van Cleave, C.D. (1929). An Experimental Study of Fission and Reconstitution in Stenostomum. Physiol. Zool. *2*, 18–58. https://doi.org/10.1086/physzool.2.1.30151062.
43. Goldsmith, E.D. (1942). Sexuality in *Dugesia tigrina* (syn. *Planaria maculata*). Nature *150*, 351. Syn Planaria maculata. https://doi.org/10.1038/150351a0.
44. Isaeva, V., Alexandrova, Y., and Reunov, A. (2005). Interaction between chromatoid bodies and mitochondria in neoblasts and gonial cells of the asexual and spontaneously sexualized planarian, Girardia (Dugesia) tigrina. Invertebr. Reprod. Dev. *48*, 119–128. https://doi.org/10.1080/07924259.2005.9652178.
45. Nuttycombe, J.W., and Waters, A.J. (1938). The American Species of the Genus Stenostomum. Proc. Am. Philos. Soc. *79*, 213–301.
46. Egger, B., Ladurner, P., Nimeth, K., Gschwentner, R., and Rieger, R. (2006). The regeneration capacity of the flatworm Macrostomum lignano–on repeated regeneration, rejuvenation, and the minimal size needed for regeneration. Dev. Genes Evol. *216*, 565–577. https://doi.org/10.1007/s00427-006-0069-4.
47. Mouton, S., Grudniewska, M., Glazenburg, L., Guryev, V., and Berezikov, E. (2018). Resilience to aging in the regeneration-capable flatworm Macrostomum lignano. Aging Cell *17*, e12739. https://doi.org/10.1111/acel.12739.
48. Mouton, S., Willems, M., Back, P., Braeckman, B.P., and Borgonie, G. (2009). Demographic analysis reveals gradual senescence in the flatworm Macrostomum lignano. Front. Zool. *6*, 15. https://doi.org/10.1186/1742-9994-6-15.
49. Tomczyk, S., Fischer, K., Austad, S., and Galliot, B. (2015). Hydra, a powerful model for aging studies. Invertebr. Reprod. Dev. *59*, 11–16. https://doi.org/10.1080/07924259.2014.927805.
50. Haluza, Y., Zoller, J.A., Lu, A.T., Walters, H.E., Lachnit, M., Lowe, R., Haghani, A., Brooke, R.T., Park, N., Yun, M.H., et al. (2024). Axolotl epigenetic clocks offer insights into the nature of negligible senescence. Preprint at bioRxiv.
51. Tan, T.C.J., Rahman, R., Jaber-Hijazi, F., Felix, D.A., Chen, C., Louis, E.J., and Aboobaker, A. (2012). Telomere maintenance and telomerase activity are differentially regulated in asexual and sexual worms. Proc. Natl. Acad. Sci. USA *109*, 4209–4214. https://doi.org/10.1073/pnas.1118885109.
52. Kang, J., Dong, Z., Wang, J., Chen, G., and Liu, D. (2019). Autophagy-related Djatg8 is required for remodeling in planarian Dugesia japonica. Biol. Open *8*, bio045013. https://doi.org/10.1242/bio.045013.
53. Ma, K., Zhang, Y., Song, G., Wu, M., and Chen, G. (2018). Identification of Autophagy-Related Gene 7 and Autophagic Cell Death in the Planarian Dugesia japonica. Front. Physiol. *9*, 1223. https://doi.org/10.3389/fphys.2018.01223.
54. Allikka Parambil, S., Li, D., Zelko, M., Poulet, A., and van Wolfswinkel, J.C. (2024). piRNA generation is associated with the pioneer round of translation in stem cells. Nucleic Acids Res. *52*, 2590–2608. https://doi.org/10.1093/nar/gkad1212.
55. Li, D., Taylor, D.H., and van Wolfswinkel, J.C. (2021). PIWI-mediated control of tissue-specific transposons is essential for somatic cell differentiation. Cell Rep. *37*, 109776. https://doi.org/10.1016/j.celrep.2021.109776.
56. Schindelin, J., Arganda-Carreras, I., Frise, E., Kaynig, V., Longair, M., Pietzsch, T., Preibisch, S., Rueden, C., Saalfeld, S., Schmid, B., et al. (2012). Fiji: an open-source platform for biological-image analysis. Nat. Methods *9*, 676–682. https://doi.org/10.1038/nmeth.2019.
57. Zayas, R.M., A.H., Habermann, B., Wang, Y., Stary, J.M., and Newmark, P.A. (2005). The planarian Schmidtea mediterranea as a model for epigenetic germ cell specification: analysis of ESTs from the hermaphroditic strain. Dev. Biol.
58. Poulet, A., Kratkiewicz, A.J., Li, D., and van Wolfswinkel, J.C. (2023). Chromatin analysis of adult pluripotent stem cells reveals a unique stemness maintenance strategy. Sci. Adv. *9*, eadh4887. https://doi.org/10.1126/sciadv.adh4887.
59. Robb, S.M.C., Gotting, K., Ross, E., and Sánchez Alvarado, A. (2015). SmedGD 2.0: The Schmidtea mediterranea genome database. Genesis *53*, 535–546. https://doi.org/10.1002/dvg.22872.
60. Cross, S.D., Johnson, A.A., Gilles, B.J., Bachman, L.A., Inoue, T., Agata, K., Marmorstein, L.Y., and Marmorstein, A.D. (2015). Control of Maintenance and Regeneration of Planarian Eyes by ovo. Invest. Ophthalmol. Vis. Sci. *56*, 7604–7610. https://doi.org/10.1167/iovs.15-17458.
61. King, R.S., and Newmark, P.A. (2013). In situ hybridization protocol for enhanced detection of gene expression in the planarian Schmidtea mediterranea. BMC Dev. Biol. *13*, 8. https://doi.org/10.1186/1471-213X-13-8.
62. Vila-Farré, M., Vu, H.T.-K., and Rink, J.C. (2023). Whole-Mount In Situ Hybridization in Large Sexual Schmidtea mediterranea. In Schmidtea Mediterranea: Methods and Protocols, L. Gentile, ed. (Springer), pp. 107–119. https://doi.org/10.1007/978-1-0716-3275-8_7.
63. Motulsky, H.J., and Brown, R.E. (2006). Detecting outliers when fitting data with nonlinear regression – a new method based on robust nonlinear regression and the false discovery rate. BMC Bioinform. *7*, 123. https://doi.org/10.1186/1471-2105-7-123.

STAR★METHODS

KEY RESOURCES TABLE

REAGENT or RESOURCE	SOURCE	IDENTIFIER
Antibodies		
Goat polyclonal anti-Rabbit IgG, HRP	Abcam	ab6721; RRID: AB_955447
Goat polyclonal anti-Mouse IgG, HRP	Abcam	ab6789; RRID: AB_955439
Bacterial and virus strains		
DH10-B	N/A	F- mcrA Δ(mrr-hsdRMS-mcrBC) Φ80dlacZΔM15 ΔlacX74 endA1 recA1 deoR Δ(ara,leu)7697 araD139 galU galK nupG rpsL λ–
Chemicals, peptides, and recombinant proteins		
Hydrogen Peroxide, 30%	Sigma Aldrich	216763-500ML
Gentamicin Sulfate	VWR	75856-638
Red Food Color, 1 Fluid Ounce	McCormick	N/A
Green Food Color, 1 Fluid Ounce	McCormick	N/A
Ampicillin, Sodium Salt	American Bio	AB00115-00010
X-Gal	Cayman Chemical Company	16495-5
Dioxane-Free Isopropyl β-D-thiogalactopyranoside (IPTG)	American Bio	AB00841-00005
4′,6-Diamidino-2-Phenylindole, dilactate (DAPI)	Invitrogen	D3571
Other lab chemicals	See methods	Unless otherwise specified, all other chemicals and reagents were obtained from Sigma Aldrich.
Experimental models: Organisms/strains		
Planaria	Sexually-reproducing S2 line	Lab stock
Oligonucleotides		
qPCR primers for RNAi validation (*gapdh, ubiquillin, histone H4, notum, beta-catenin, dmd-1, wnt5, wntA*)	This paper; see Table S1.	N/A
Primers for generation of dsRNA and riboprobes (*unc-22*, *notum, beta-catenin, dmd-1, wnt1 wnt5, wntA*)	For *unc*-22, see Li et al. (2021).[55] For all others, this paper; see Table S1.	N/A
Recombinant DNA		
pGEM-T	Promega	A3600
pGEM-*unc22*	Li et al., 2021[55]	N/A
pGEM-*notum*	This paper	N/A
pGEM-*wnt1*	This paper	N/A
pGEM-*wnt5*	This paper	N/A
pGEM-*wntA*	This paper	N/A
pGEM-*dmd-1*	This paper	N/A
pGEM-*beta-catenin*	This paper	N/A
Software and algorithms		
ImageJ version 1.52q	Schindelin et al. 2012[56]	https://imagej.net/ij/
GraphPad Prism	GraphPad Software	https://www.graphpad.com/scientific-software/prism/
Planarian Image Quantification (PIQ) package v1.0.7	Allikka Parambil et al. 2024[54]	https://gitlab.com/vanwolfswinkel/PIQ

EXPERIMENTAL MODEL AND STUDY PARTICIPANT DETAILS

Planarian culture and husbandry

All experiments were performed using the S2 hermaphroditic strain of *S. mediterranea*, which was maintained as described previously.[9,17,55,57] Briefly, animals were cultured in the dark at 20 degrees Celsius in deionized water supplemented with 1x Montujïch salts and 0.05 mg/mL gentamicin sulfate to prevent infection. Unless otherwise specified, animals were fed organic cow liver paste weekly, and water was exchanged both immediately after and 2-3 days following each feed to ensure organismal health. Animals were monitored weekly to isolate egg capsules and identify injured planarians (which were removed from the experiment and allowed to recover separately). Egg capsules were cultured for at least 28 days using the same water used to culture mature planarians, and were checked for hatchlings weekly, which were isolated and raised in age-matched cohorts. Amputations were performed transversely through the pharynx using a razor blade, and anterior and posterior fragments were separated, cleaned twice weekly, and starved for 21 days to facilitate recovery: any animals that failed to form a blastema by day 21 were removed from the experiment and allowed to recover separately. Based upon the data presented in Figures 1 and S1, we defined "young" planarians as animals that had hatched from egg capsules, were between 56 and 77 days of age, and possessed a visible gonopore (indicating the presence of a functional reproductive system.) We defined "regenerated" planarians as animals that had regenerated from an amputated tail fragment (unless otherwise specified), were between 56 and 77 days of age after amputation, and possessed a visible gonopore. We defined "aged" planarians as animals that were at least 120 days beyond hatching or last regeneration event, and which had not produced any viable hatchlings for at least 28 days. All animals (unless otherwise specified) were cocultured with other animals of the same age and cohort, and freely allowed to copulate.

METHOD DETAILS

Heterochronic and synchronic mating experiments

Young, aged, and regenerated planarians (from head fragments) were randomly selected and assigned to heterochronic or synchronic conditions, paired together, and housed in 3 cm^2 petri dishes. Immediately prior to pairing, each animal was fed cow liver mixed with either red or green food coloring, allowing the two animals to be distinguished from each other due to differences in color. Animals were paired for 3 days, then isolated from each other into separate 3 cm^2 dishes. Capsules produced by these animals in isolation were collected and quantified over the next 4 days, and monitored for hatchling production over the next four weeks. Animals were then re-paired the next week with a different randomly-selected animal in the appropriate experimental cohort, eliminating batch effects that may occur due to pairing an infertile animal with a fertile partner. This process was repeated until the end of fertility (over the course of 5-6 weeks). Animals that became injured or were unable to be distinguished from their partner were removed from the experiment and excluded from subsequent matings.

RNA interference

RNA interference was accomplished as described previously[58] by administration of in-vitro-synthesized dsRNA. Briefly, 0.5-2 kB regions of genes of interested were identified through bioinformatic analysis,[59] then amplified from bulk cDNA using sequence-specific PCR primers (See Table S1). These products were then cloned into the Promega pGEM-T vector system and validated through Sanger sequencing. After the addition of an adapter sequence (TAATACGACTCACTATA) for T7 RNA polymerase, forward and reverse ssRNA copies of each construct were generated, which were hybridized together at 37 degrees for 30 minutes to form dsRNA. Both ssRNA and dsRNA constructs were validated using gel electrophoresis. dsRNA against each gene was mixed with red food coloring and organic cow liver paste at a 2:3:50 ratio for feeding. Animals were fed twice weekly; any animals that went one week without eating were removed from the experiment. RNAi efficacy was validated both through qPCR and (where appropriate) characterization of obvious physiological defects. Animals were starved for at least 1 week before fixation to ensure that no food would remain in the intestines and interfere with the imaging process.

For long-term fertility tracking experiments (Figures 6 and S6–S7), dsRNA treatment was performed on cohorts of 6-10 randomly-selected regenerated animals, beginning at the start of the animals' fertility windows (day 57-65 after amputation) and maintained through the end of said window. Two metrics were used to assay organismal fertility: fertile period length (defined for each cohort as the number of weeks between the first and last production of hatchlings) and average weekly fertility per animal. Due to low fertility in RNAi-treated animals, both animals treated with RNAi against *unc-22* (a *C. elegans* gene that has no planarian homologue)[60] and untreated animals are presented as controls. Animals were fixed at 39-41 days after their first feed for fluorescent in situ hybridization to assay the reproductive system at peak fertility. Due to severe polarity defects that interfered with feeding behavior, *beta-catenin* RNAi and age-matched control animals were instead harvested prematurely at 29-31 days after their first feed. For *dmd-1* RNAi treatment (Figures S5L–S5R), sexually-mature regenerated planarians were treated with dsRNA against *dmd-1* or *unc-22* for 6 weeks before fixation and staining for the ovarian marker *lecg*. For *wntA* and *wnt5* RNAi (Figure S7X), animals were treated for 39 days (*wnt5*+control) or 84 days (*wntA*+control).

Fluorescent in situ hybridization

Fluorescent in Situ Hybridization (FISH) was performed on planarians as described previously,[61] with modifications to accommodate the large size of many of the animals.[62] Briefly, animals were gently demucinated through consecutive incubations in pH 7 0.5% NAC

buffered with 20 mM HEPES followed by 7.5% NAC; fixed in 4% formaldehyde; permeabilized using 1% SDS/NP40 and 5 mM DTT; and bleached of pigment using 1.5% H2O2 in 5% formamide. Fixed animals were then treated with 2μg/mL proteinase K before being incubated with dioxygenin (DIG) or fluorescein (Fl)-labelled ssRNA probes, generated using the same procedure as described in the RNA interference protocol above (see Table S1 for primer details) and dissolved in formamide. Animals were then washed using consecutive incubations in prehyb solution, 1:1 prehyb mixed with 2x SSC, 2x SSC, 0.2x SSC, and 0.05x SSC. Probes were detected using Roche anti-DIG-POD or anti-Fl-POD antibodies in combination with tyramide signal amplification. Excess tyramide was quenched through inactivation with 1% NaN_3. Animals were counterstained with the DNA-binding dye 4′,6-diamidino-2-phenylindole (DAPI).

Image scoring and quantification

After FISH, animals were imaged by widefield fluorescent microscopy using a Leica M165 FC or by confocal microscopy using a Zeiss LSM800. Confocal images of ovaries were taken at 20x magnification at a voxel size of 0.35x0.35x4.5 μm (except for *beta-catenin* RNAi images and their controls, which due to the greater area over which the ovaries were spread, were taken at 10x magnification at a voxel size of 0.69x0.69x11 μm), and processed into a maximum projection using the ImageJ software tool version 1.52q.[56] Confocal images of testes (Figure S5I) were taken at a resolution of 0.13 μm x 0.13 μm x 4.5 μm (young), 0.11μm x 0.11μm x 4.5 μm (aged), and 0.10 μm x 0.10 μm x 4.5 μm (regenerated) respectively. Unless otherwise stated, scale bars on all images represent 50 μm.

For ovarian counts of large numbers of animals (Figures 2C and S2A), images were automatically quantified using the planarian image quantification program (PIQ)[54] using the configuration file contained in Data S1A. For counts in smaller numbers of animals (Figures 6F, 6G, S5M, S7A, and S7J), widefield fluorescent images were taken, blinded, and scored manually. For oocyte quantifications (Figure 2D), a similar approach was applied to confocal fluorescent stacks to more accurately visualize and quantify the oocytes. For all quantifications, in order to control for variation in organismal size, data are also presented normalized to the length and width of the brain (Figures S2A, S2B, S5N, S5O, S7B–S7E, S7K, and S7L). In these animals, the brain was visualized by staining with DAPI. Brain length was measured from the posterior tip of the base of each lobe of the brain to the anterior tip of the animal using ImageJ's built-in distance measurement tool; these measurements were then averaged per animal. Brain width was measured as the widest distance between the brain lobes. Total and average ovarian area (Figures 6H and S7F) was automatically quantified using the planarian image quantification program (PIQ)[54] using the configuration file contained in Data S1B. For ovarian cell composition in animals of different ages (Figure 3C), confocal fluorescent stacks of ovaries were cropped to isolate individual ovaries, which were scored manually for the presence of early and late oocytes based on size, shape, and position within the ovary, based upon previous observations.[23] A similar approach was applied to study the composition of anterior, posterior, and single ovaries in aged animals (Figure 3F). These ovaries were grouped based on their organization within the flank of the animal: single ovaries (i.e. no other ovaries were present on the same side of the animal), anterior ovaries, or posterior ovaries. Ovaries that had more than one other neighbor on the same flank of the animal, that overlapped along the anterior-posterior axis, or that were only one cell in size were excluded from these analyses.

For organismal size quantifications (Figure S3), animals were stained with DAPI to visualize them under widefield fluorescence microscopy. These images were automatically scored for fluorescent area using ImageJ's built-in threshold function, and manually scored for their length (from anterior to posterior tips) and width (defined as the longest distance from left to right that passes through the pharynx) (presented in Figure S3B). Histograms were generated by determining the total range in area, length, or width from all animal cohorts aggregated, and splitting this into 20 bins of equal size; the histograms in Figure S3C, S3F, and S3I show the number of animals within each bin. For the scatter plots (Figure S3D, S3G, and S3J), a simple linear regression was fitted between the number of ovaries and each of these measures of organismal size in young, aged, and regenerated conditions. Outliers were detected using GraphPad Prism's inbuilt ROUT method[63] at the recommended stringency of Q=1%, and were excluded from the final graphs. Exclusion of these outliers did not affect the significance of the results. For comparison of the number of ovaries per animal in organisms of comparable area (Figure S3E), for each pairwise comparison (i.e. aged vs. young, aged vs. regenerated, and young vs. regenerated), a range of areas was defined that overlapped both groups. For example, the range of areas in Figure S3C is 0.026 cm^2-0.15 cm^2 in young animals, while the range of areas in aged animals is 0.082 cm^2-0.24 cm^2; as such, we defined animals in both groups between 0.082-0.15 cm^2 to be of comparable size, and used them for the analysis in Figure S3E. A similar approach was employed for organismal length in Figure S3H and organismal width in Figure S3K.

For germ cell progenitor quantifications (Figures 3G, 3I, 3J, 6U, 6V, and S7P–S7R), the region around each ovary was imaged using confocal fluorescent stacks. We detected the number of GCPs using the PIQ software tool (see Data S1C and S1D), defined a region of 30 μm around each ovary, and detected the number of cells contained therein.[54] Cells within this region ("proximal GCPs") were assumed to be exclusively associated with that ovary, while all other cells were defined as distal GCPs. Since proximal GCPs are associated with specific ovaries while distal GCPs are not, data for proximal GCPs is normalized to the number of ovaries, while data for distal and total GCPs is normalized on a per-animal basis. The reciprocal normalizations (Figures S4A–S4C, S7P–S7R) can be found in supplemental figures, as can normalizations to brain length and width (see above). Any animals where one or more ovaries could not be clearly imaged were excluded from this analysis. For germ cell progenitor quantifications in *beta-catenin* RNAi and control animals (Figures 6N–6P, S7G, and S7H), images were taken of the region anterior to and posterior to the most anterior set of ovaries. The images were then cropped to eliminate overlap, and the total number of GCPs in each region were computed using PIQ as described above (see Data S1B). For quantifications of the GCPs in the region anterior to the ovaries (Figures 3L and 6W), for each ovary, we cropped the image through the midline of the ovary as a posterior boundary. For posterior ovaries, for the

anterior boundary, we cropped the images through the midline of the ovary above; for all other images, we cropped the image at the anterior end of the spray of *notum+* GCPs. We then blinded and hand-scored the number of GCPs anterior to each ovary, classified the ovaries by whether they were anterior, posterior, or single (as above) and normalized them to brain length and width in supplementary figures (Figures S4D, S7G, S7H, S7S, and S7T).

For ovarian disconnection quantification (Figures 4C), confocal fluorescent images were blinded, then each ovary was scored for the presence of an oviduct and a tuba. The percentage of ovaries that lacked either of these two essential structures was then computed. A similar approach was used for Figure 4E, which first classified ovaries as anterior, posterior, or single (see above), before scoring whether they lacked connections. Figures 6R and S7V scored individual animals based on the percentage of ovaries that were connected; Figure S7W also fractionated ovaries based on their position. Owing to the unique distribution of ovaries in *b-catenin* RNAi animals, Figure 6S separately examined the percent connectivity of the anteriormost vs. posterior ovaries in *beta-catenin* and control RNAi animals.

For quantification of ovarian niche circlets (Figures S4G and S4H), confocal fluorescent images were blinded, then each ovary was scored for the presence of niche circlets.

For quantification of *notum+* (Figures 5C, S5B, and S5C) and *wnt1+* (Figures S4F and S4G) pole cells, confocal fluorescent images were automatically quantified using the planarian image quantification software (PIQ)[54] with configuration files provided in Data S1E and S1F. For both *notum* and *wnt1*, in addition to the raw number of cells, a quantification of the area over which these cells are spread is provided, which was calculated by defining the minimum retangular area that contains all foci.

For quantification of normalized ovarian distances (Figures 2F–2H, 6I–6K, S5P–S5R, and S7M–S7O), widefield fluorescent images were taken, then the distance between each ovary and the anterior tip of the animal was measured using ImageJ's built-in distance measurement tool. To normalize this distance for variation in organismal size, ovarian distances were divided by the average distance between each eye and the anterior tip of the animal, which were also measured using widefield fluorescent staining for DAPI in ImageJ. As a further validation of this normalization approach, we also normalized overall, maximum, and minimum ovarian distances in aged, young, and regenerated animals to brain length (Figure S2C) and width (Figure S2D) in supplementary figures.

For quantification of normalized posterior distance (Figure S5H), the distance between the ovaries and the posterior tip of the animal was divided by the width of the animal through the pharynx to control for variation in organismal size. All distances were measured using widefield fluorescent images through DAPI staining in ImageJ.

For quantification of valley length (Figure S5K), the distance between the eyes and the anterior tip of the animal was subtracted from the distance between anteriormost set of testes and the anterior tip of the animal to yield the distance between the eyes and the anteriormost set of testes, which is the region in which the ovaries develop. This distance was then normalized to organismal size by dividing by the organismal width through the pharynx. All distances were measured using widefield fluorescent images through DAPI staining in ImageJ.

QUANTIFICATION AND STATISTICAL ANALYSIS

For all categorical data where statistical significance was computed (Figures 1I, 1J, 3C, 3F, 4C, and 4E), Fisher's exact test was used to compute p-values. For all other data where statistical significance was computed, a Kolmogorov-Smirnov test was first used to determine if the data were normally distributed. For normally distributed data, ANOVA was used to determine if there was a statistically-significant difference among any groups, then Welch's T-test was used to compute p-values between individual groups. For data that were not normally distributed, the non-parametric Kruskal-Wallis test was used to determine if there was a statistically-significant difference among any groups, then the non-parametric Mann-Whitney U-test was used to compute p-values between groups. All data were graphed using the GraphPad Prism software tool version 10.2.2.

Current Biology, Volume *36*

Supplemental Information

Drift of positional identity drives reproductive aging in a long-lived regenerative animal

Andrew Verdesca, Axel Poulet, Maxwell Bales, and Josien C. van Wolfswinkel

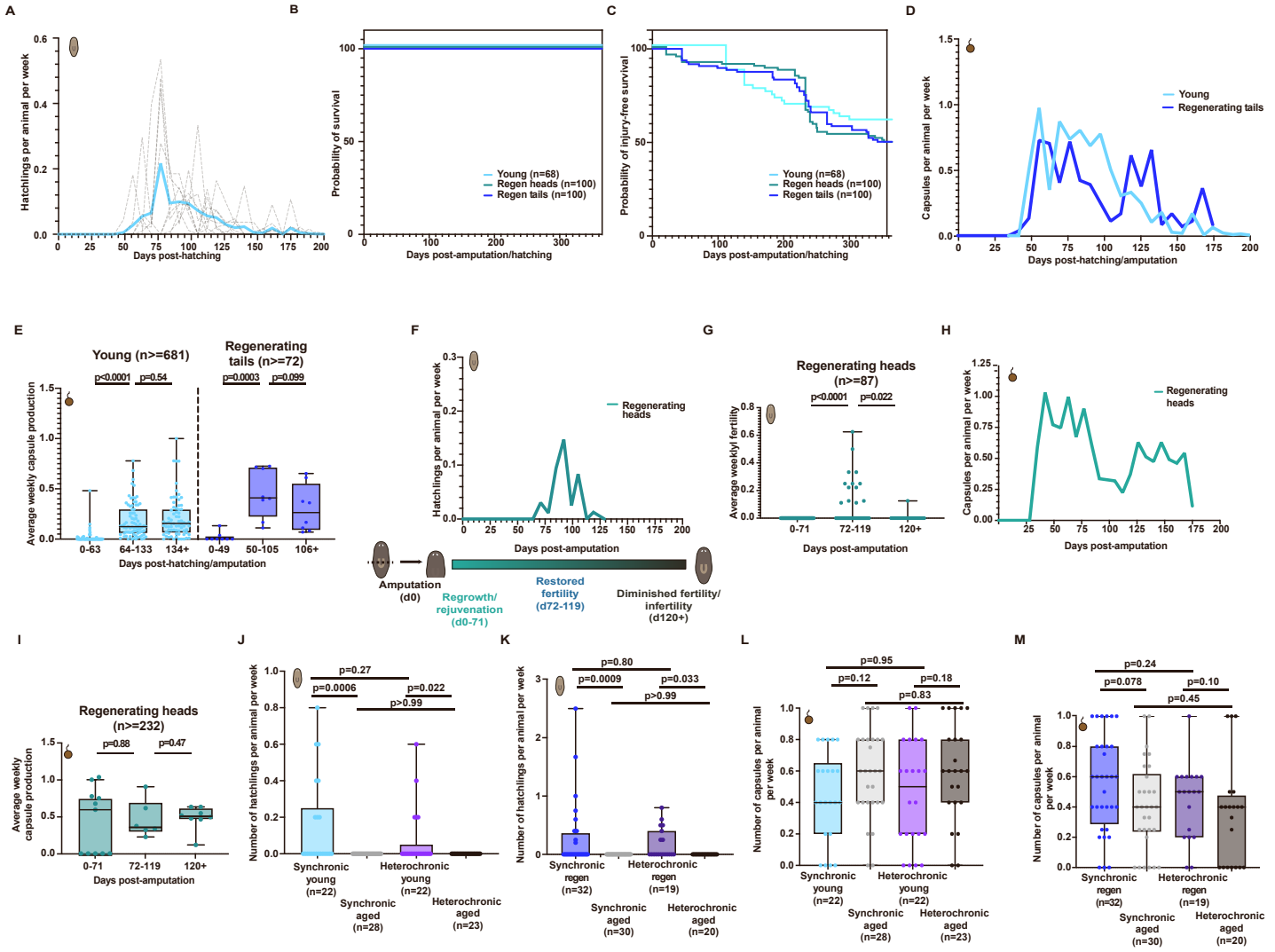

Figure S1. Additional fertility data of aging and regenerating planarians.
Related to Figure 1.

(A) Fertility curves of the eight cohorts of animals averaged in Figure 1b. Each grey line represents the fertility of an individual cohort, while the teal line represents the average fertility across all cohorts. **(B)** Survival curve showing the probability of mortality during the first year of life across cohorts of young intact planarians, regenerating head fragments, and regenerating tail fragments. **(C)** Injury-free survival curve showing the probability of injury during the first year of life across cohorts of young intact planarians, regenerating head fragments, and regenerating tail fragments. **(D)** Capsule-production curve showing the number of capsules produced by young and regenerating tail fragments over the course of the first 175-200 days of their lives. For young planarians, the capsule-production curve displays the average of eight cohorts of between 27 and 136 planarians, and reflects the number of capsules produced by each cohort each week normalized to the number of animals in that cohort. Data for the regenerating tail fragments is derived from a cohort of 232 planarians, and reflects the number of capsules produced each week normalized to the number of animals in the cohort. **(E)** Quantification of capsules produced during aging and regeneration. Average weekly capsule data from young animals was binned into 9-week segments representing growth/maturation, fertility, and diminished fertility. Average weekly capsule data from regenerated animals was binned into an 8-week regrowth/rejuvenation phase, an 8-week restored fertility phase, and a terminal diminished fertility phase. P-values were computed using a Mann-Whitney U Test. **(F)** Fertility curve showing the number of hatchlings produced by regenerating head fragments over the course of the first 130 days of their lives. The fertility curve displays the number of hatchlings produced by 11 cohorts of 9 planarians, and reflects the number of hatchlings produced each week normalized to the number of animals in each cohort. **(G)** Quantification of hatchlings produced during regeneration in head fragments. Average weekly fertility data from each cohort was binned into an 11-week regrowth/ rejuvenation phase, a 6-week restored fertility phase, and a diminished fertility phase. P-values were computed using a Mann-Whitney U Test. **(H)** Capsule-production curve showing the number of capsules produced by regenerating head fragments over the course of the first 130 days of their lives. The data is derived from a cohort of 232 planarians, and reflects the number of capsules produced each week normalized to the number of animals in the cohort. **(I)** Quantification of

capsules produced during regeneration in head fragments. Average weekly capsule data from the cohort was binned into an 11-week regrowth/rejuvenation phase, a 6-week restored fertility phase, and a diminished fertility phase. P-values were computed using a Mann-Whitney U Test. **(J)** Average weekly fertility of individual synchronic young, synchronic aged, and (separately) the aged and young members of heterochronic pairs over the course of five weeks starting one week after the young animals reached fertility. P-values were computed using a Mann-Whitney U Test. **(K)** Average weekly fertility of individual synchronic regenerated, synchronic aged, and (separately) the aged and regenerated members of heterochronic pairs over the course of six weeks starting one week after the regenerated animals reached fertility. Regenerated head fragments were used for this analysis. P-values were computed using a Mann-Whitney U Test. **(L)** Average weekly capsule production of individual synchronic young, synchronic aged, and (separately) the aged and young members of heterochronic pairs over the course of 5 weeks starting one week after the young animals reached fertility. P-values were computed using a Mann-Whitney U Test. **(M)** Average weekly capsule production of individual synchronic regenerated, synchronic aged, and (separately) the aged and regenerated members of heterochronic pairs over the course of 6 weeks starting one week after the regenerated animals reached fertility. Regenerated head fragments were used for this analysis. P-values were computed using a Mann-Whitney U Test. Error bars of boxplots represent minimum and maximum observations.

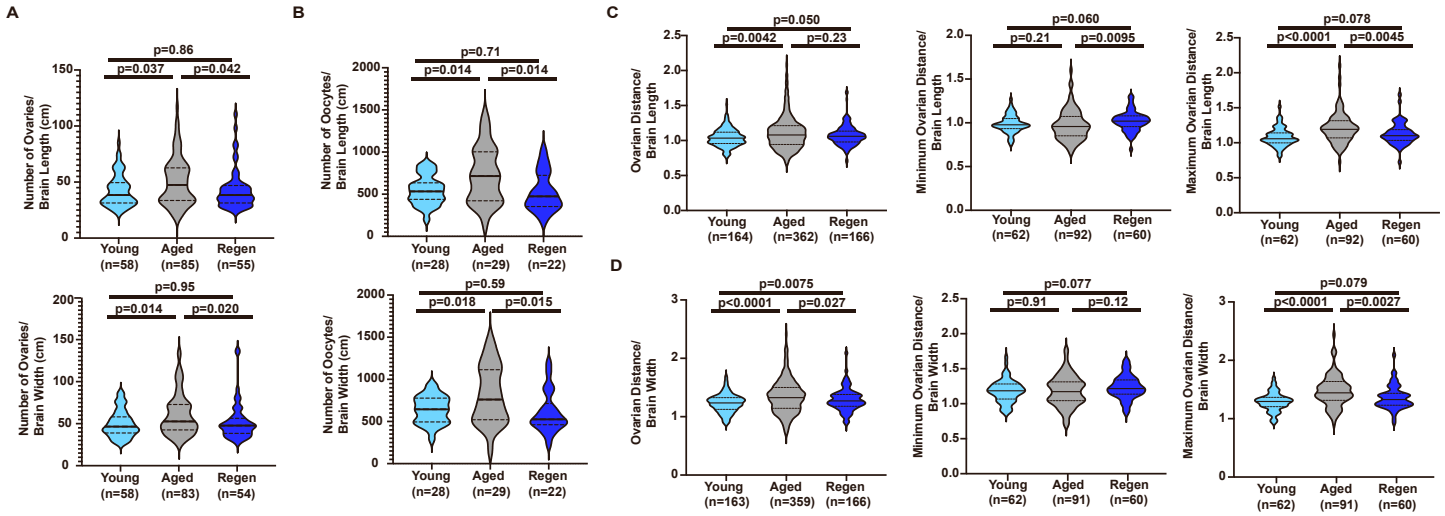

Figure S2. Additional normalization of ovarian counts and ovarian distance.
Related to Figure 2.
(A) Quantification of the number of ovaries per animal normalized to brain length (top) and width (bottom) in young, aged, and regenerated animals. P-values were computed using a Mann-Whitney U Test. **(B)** Quantification of the number of oocytes per animal normalized to brain length (top) and width (bottom) in young, aged, and regenerated animals. P-values were computed using Welch's T-test. **(C)** Quantification of the overall (left) minimum (center) and maximum (right) ovarian distance normalized to brain length in young, aged, and regenerated animals. P-values were computed using a Mann-Whitney U-Test. **(D)** Quantification of the overall (left) minimum (center) and maximum (right) ovarian distance normalized to brain width in young, aged, and regenerated animals. P-values were computed using a Mann-Whitney U-Test (overall and maximum ovarian distance) or Welch's T-Test (minimum ovarian distance). Solid lines on violin plots indicate medians, and dotted lines indicate quartile boundaries.

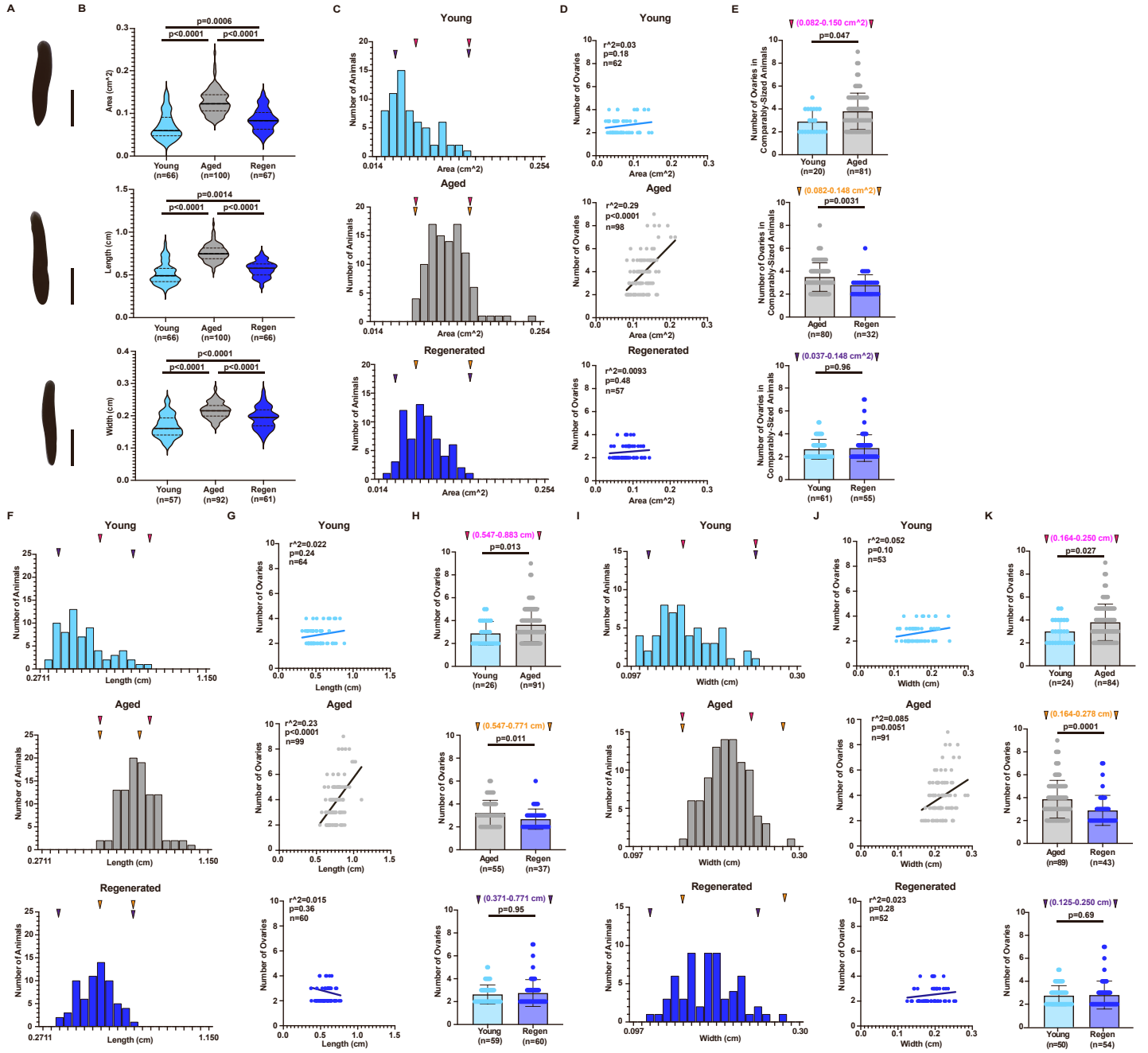

Figure S3. Information on animal sizes and ovarian counts in the various cohorts. Related to Figure 2.

(A) Images of a young (top), aged (middle), and regenerated (bottom) planarian. Scale bar = 0.5 cm. **(B)** Quantification showing three different measures of organismal size in young, aged, and regenerated animals: fluorescent area by DAPI (top), length (middle), and width (bottom). P-values were calculated using a Mann-Whitney U Test for area and length, and Welch's T-Test for width. Solid lines on violin plots indicate medians, and dotted lines indicate quartile boundaries. **(C)** Histograms showing the distribution of organismal area in young, aged, and regenerated animals. Magenta arrowheads indicate organisms of comparable area between aged and young animals used in Figure S3E (top), orange arrowheads indicate organisms of comparable area between aged and regenerated animals used in Figure S3E (middle), and purple arrowheads indicate organisms of comparable area between young and regenerated animals used in Figure S3E (bottom). **(D)** Scatter plot showing the relationship between organismal area and the number of ovaries in young (top), aged (middle), and regenerated (bottom) animals. **(E)** Quantification of the number of ovaries per animal in animals of comparable areas: young vs. aged (top), aged vs. regenerated (middle), and young vs. regenerated (bottom). P-values were calculated using a Mann-Whitney U Test. **(F)** Histograms showing the distribution of organismal length in young, aged, and regenerated animals. Magenta arrowheads indicate organisms of comparable length between aged and young

animals used in Figure S3H (top), orange arrowheads indicate organisms of comparable length between aged and regenerated animals used in Figure S3H (middle), and purple arrowheads indicate organisms of comparable length between young and regenerated animals used in Figure S3H (bottom). **(G)** Scatter plot showing the relationship between organismal length and the number of ovaries in young (top), aged (middle), and regenerated (bottom) animals. **(H)** Quantification of the number of ovaries per animal in animals of comparable lengths: young vs. aged (top), aged vs. regenerated (middle), and young vs. regenerated (bottom). P-values were calculated using a Mann-Whitney U Test. **(I)** Histograms showing the distribution of organismal width in young, aged, and regenerated animals. Magenta arrowheads indicate organisms of comparable width between aged and young animals used in Figure S3K (top), orange arrowheads indicate organisms of comparable width between aged and regenerated animals used in Figure S3K (middle), and purple arrowheads indicate organisms of comparable width between young and regenerated animals used in Figure S3K (bottom). **(J)** Scatter plot showing the relationship between organismal width and the number of ovaries in young (top), aged (middle), and regenerated (bottom) animals. **(K)** Quantification of the number of ovaries per animal in animals of comparable widths: young vs. aged (top), aged vs. regenerated (middle), and young vs. regenerated (bottom). P-values were calculated using a Mann-Whitney U Test. Error bars of bargraphs represent standard deviations.

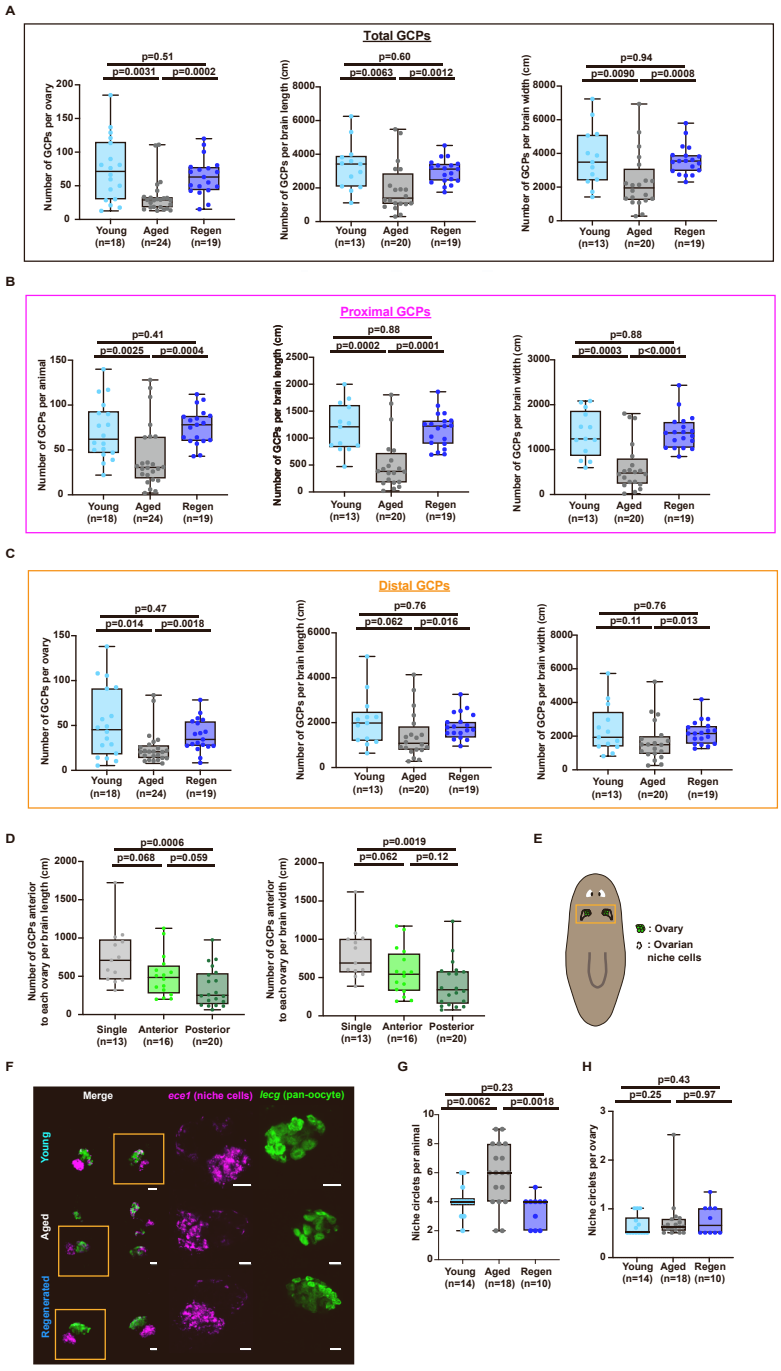

Figure S4. Additional normalizations of ovarian attributes.
Related to Figure 3.

(A) Quantification of total germ cell progenitors per ovary (left), brain length (center), and brain width (right) in young, aged, and regenerated animals. P-values were computed using a Mann-Whitney U Test. **(B)** Quantification of proximal germ cell progenitors per animal (left), brain length (center), and brain width (right) in young, aged, and regenerated animals. P-values were computed using a Mann-Whitney U Test. **(C)** Quantification of distal germ cell progenitors per ovary (left), brain length (center), and brain width (right) in young, aged, and regenerated animals. P-values were computed using a Mann-Whitney U Test. **(D)** Quantification of the number of germ cell progenitors above single, anterior, and posterior ovaries of aged animals normalized to brain length (left) or brain width (right). P-values were calculated using a Mann-Whitney U Test. **(E)** Schematic showing the expected location of the ovarian niche. **(F)** (Left): Representative widefield FISH images from young, aged, and regenerated animals, showing the pan-oocyte marker *lecg* in green and the ovarian niche marker *ece1* in magenta. (Right): Zoomed-in, confocal projections of *lecg* and *ece1* staining in the same ovaries. Note that the regenerated image used here is from the same animal as in Figure 2B. Scale bar=50 μm. **(G)** Quantification of niche circles per animal in young, aged, and regenerated animals. P-values were computed using a Mann-Whitney U Test. **(H)** Quantification of niche circles per ovary in young, aged, and regenerated animals. P-values were computed using a Mann-Whitney U Test. Error bars of boxplots represent minimum and maximum observations.

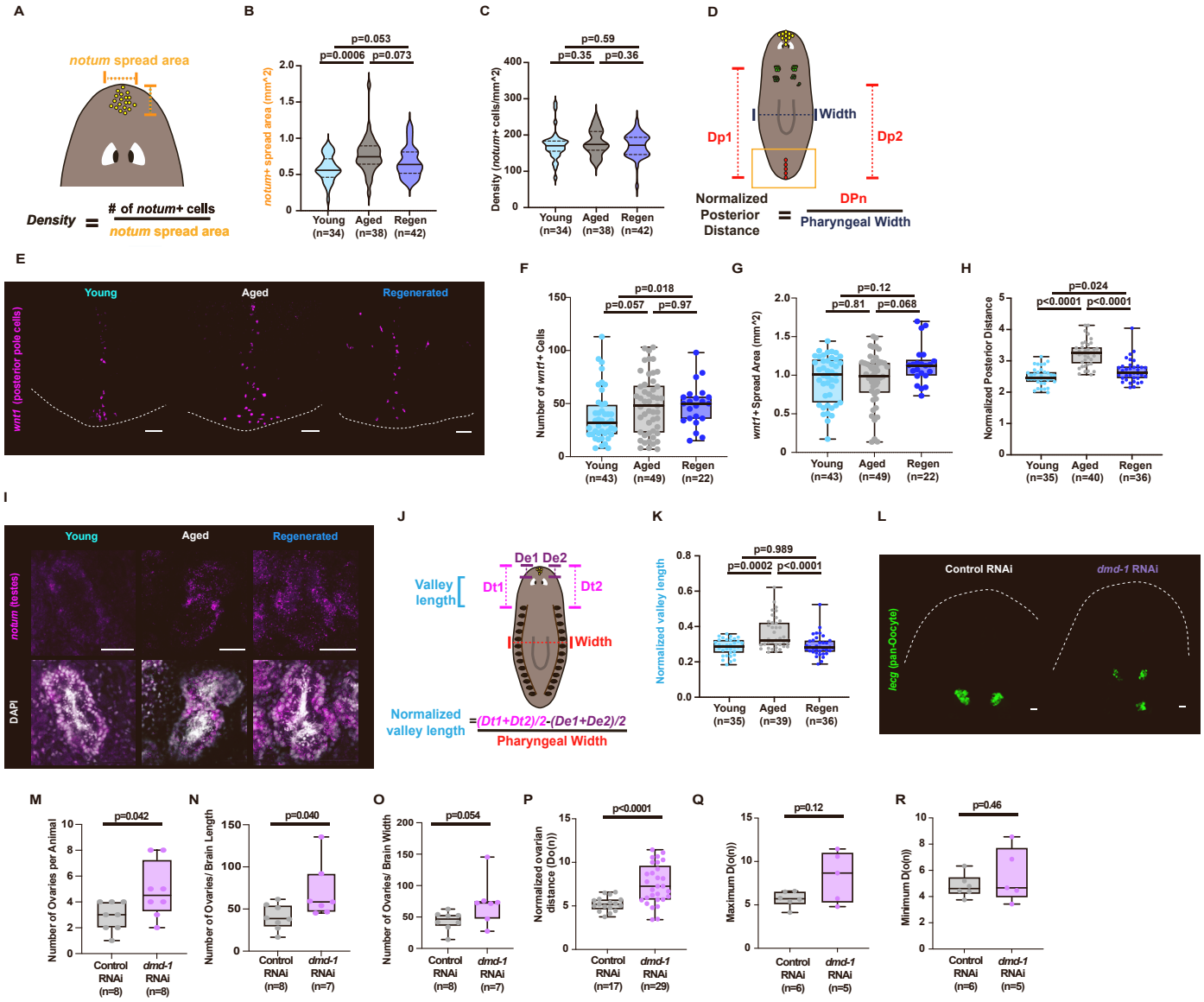

Fig. S5. Additional data on changes in Wnt signaling components with age. Related to Figure 5.

(A) Schematic showing how *notum* spread area and density were calculated. **(B)** Quantification of *notum* spread area in young, aged, and regenerated planarians. P-values were calculated using Welch's T-Test. **(C)** Quantification of *notum* spread density in young, aged, and regenerated planarians. P-values were calculated using a Mann-Whitney U Test. **(D)** Schematic showing the expected location of the *wnt1*+ posterior pole cells, and how normalized posterior distance was calculated. **(E)** Representative confocal projections of FISH images from the tails of young, aged, and regenerated animals, showing the posterior pole cell marker *wnt1* in magenta. Scale bar=50 μm. **(F)** Quantification of the number of *wnt1*+ posterior pole cells in young, aged, and regenerated animals. P-values were calculated using a Mann-Whitney U Test. **(G)** Quantification of the *wnt1*+ spread area in young, aged, and regenerated animals. P-values were calculated using a Mann-Whitney U Test. **(H)** Quantification of normalized posterior distance in young, aged, and regenerated animals. P-values were calculated using a Mann-Whitney U Test. **(I)** Previous studies [S1] have shown that *notum* is also expressed in the planarian testes. As such, we assayed whether testes in planarians of all ages expressed *notum*. This panel depicts representative confocal planes of a testis from the anterior regions of young, aged, and regenerated animals, showing *notum* expression in magenta. DAPI staining is used to show the structure of the testis, with the tightly-packed mature sperm at the center and less differentiated *notum*+ cells around the periphery. **(J)** Since the ovaries and GCPs develop in the region between two *notum*-producing populations (the testes and the anterior pole), we sought to determine if this region expands during aging by computing a metric called "normalized valley length." This metric represents the distance between the testes and the eyes normalized to organismal width, and is calculated as per this schematic. **(K)** Quantification of normalized valley length in young, aged, and regenerated animals. P-values were calculated using a Mann-Whitney U Test. **(L)** To ablate the testicular source of *notum* and increase normalized valley length, we performed RNAi against the

testicular niche gene *dmd-1*, which has previously been shown to deplete the testes without directly affecting the ovaries [S2]. This panel depicts representative widefield FISH images from control (left) and *dmd-1* RNAi (right) treated animals, showing the pan-oocyte marker *lecg* in green. Scale bar=50 μm. **(M)** Quantification of the number of ovaries per animal in control and *dmd-1* RNAi-treated animals. P-values were calculated using Welch's T-Test. Formation of ectopic ovaries in *dmd-1* RNAi-treated animals is consistent with observations in previous studies [S2], however, given that previous data has shown that the Wnt transducer gene *beta-catenin* is not elevated in the region surrounding the testes [S1], it is unclear whether these results are mediated by Wnt signaling or not. **(N)** Quantification of the number of ovaries normalized to brain length in control and *dmd-1* RNAi-treated animals. P-values were calculated using a Mann-Whitney U Test. **(O)** Quantification of the number of ovaries normalized to brain width in control and *dmd-1* RNAi-treated animals. P-values were calculated using a Mann-Whitney U Test. **(P)** Quantification of the normalized ovarian distance for each ovary in control and *dmd-1* RNAi-treated animals. P-values were calculated using Welch's T-Test. **(Q)** Quantification of the maximum normalized ovarian distance (representing the posteriormost set of ovaries) in control and *dmd-1* RNAi-treated animals. P-values were calculated using Welch's T-Test. **(R)** Quantification of the minimum normalized ovarian distance (representing the anteriormost set of ovaries) in control and *dmd-1* RNAi-treated animals. P-values were calculated using Welch's T-Test. Error bars of boxplots represent minimum and maximum observations. Solid lines on violin plots indicate medians, and dotted lines indicate quartile boundaries.

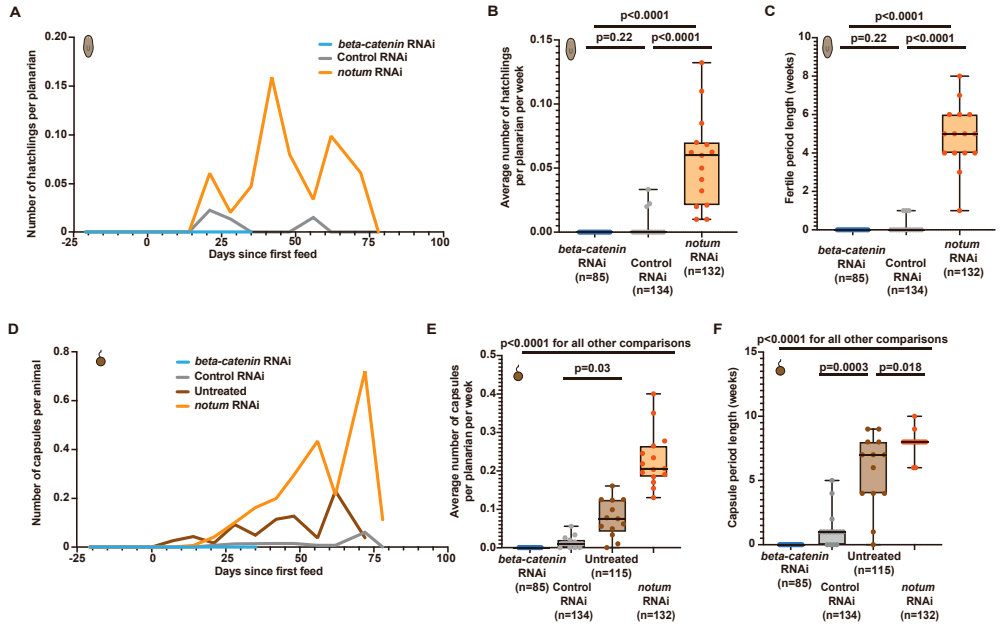

Fig. S6. Additional information on fertility of Wnt-related RNAi conditions. Related to Figure 6.

(A) Fertility curve showing the number of hatchlings produced by regenerated animals 21 days before and 77 days after treatment with either *beta-catenin* RNAi, control RNAi, or *notum* RNAi. The fertility curve displays the average of between 13-15 cohorts of 6-10 planarians each, and reflects the number of hatchlings produced by each cohort each week normalized to the number of animals in that cohort. (These data are the same as the data presented in Figure 6B, but compared to a control RNAi treatment). **(B)** Quantification of the average number of hatchlings produced each week after treatment with *beta-catenin* RNAi, control RNAi, or *notum* RNAi. (These data are the same as the data presented in Figure 6C, but compared to a control RNAi treatment). P-values were calculated using a Mann-Whitney U Test. **(C)** Quantification of the time elapsed between the first and last hatchling laid after treatment with *beta-catenin* RNAi, control RNAi, or *notum* RNAi. (These data are the same as the data presented in Figure 4D, but compared to a control RNAi treatment). P-values were calculated using a Mann-Whitney U Test. **(D)** A capsule production curve showing the number of capsules laid by regenerated animals 21 days before and 77 days after treatment with either *beta-catenin* RNAi, control RNAi, no treatment, or *notum* RNAi. The curve displays the average number of capsules produced each week by between 13-15 cohorts of 6-10 planarians each, normalized to the number of animals in that cohort. **(E)** Quantification of the average number of capsules produced each week after treatment with *beta-catenin* RNAi, control RNAi, no treatment, or *notum* RNAi. P-values were calculated using a Mann-Whitney U Test. **(F)** Quantification of the time elapsed between the first and last capsule laid after treatment with *beta-catenin* RNAi, control RNAi, no treatment, or *notum* RNAi. P-values were calculated using a Mann-Whitney U Test. Error bars of boxplots represent minimum and maximum observations.

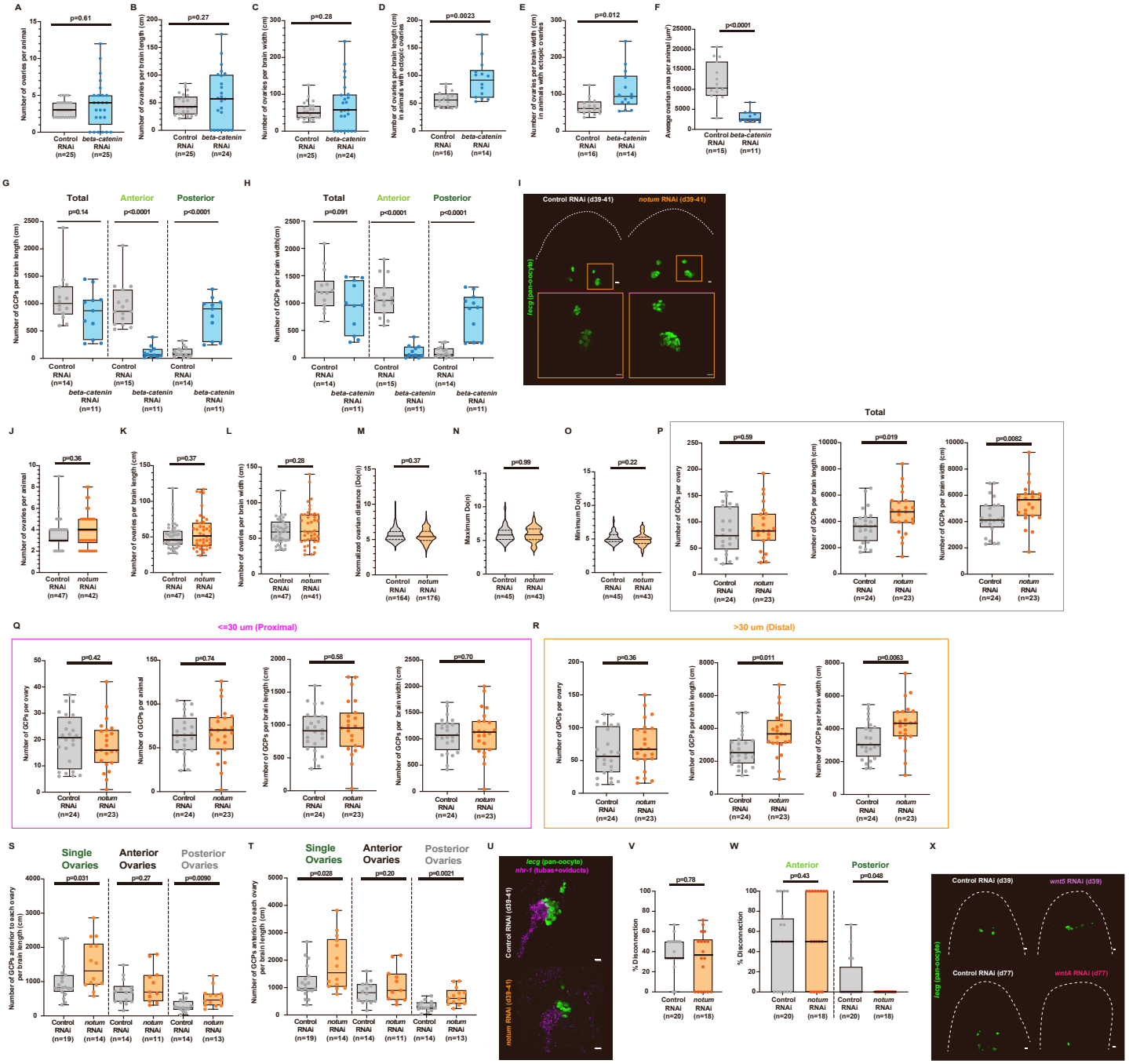
A
p=0.61
Number of ovaries per animal
Control RNAi (n=25)
beta-catenin RNAi (n=25)
B
p=0.27
Number of ovaries per brain length (cm)
Control RNAi (n=25)
beta-catenin RNAi (n=24)
C
p=0.28
Number of ovaries per brain width (cm)
Control RNAi (n=25)
beta-catenin RNAi (n=24)
D
p=0.0023
Number of ovaries per brain length (cm) in animals with ectopic ovaries
Control RNAi (n=16)
beta-catenin RNAi (n=14)
E
p=0.012
Number of ovaries per brain width (cm) in animals with ectopic ovaries
Control RNAi (n=16)
beta-catenin RNAi (n=14)
F
p<0.0001
Average ovarian area per animal (µm²)
Control RNAi (n=15)
beta-catenin RNAi (n=11)
G
Total
Anterior
Posterior
p=0.14
p<0.0001
p<0.0001
Number of GCPs per brain length (cm)
Control RNAi (n=14)
beta-catenin RNAi (n=11)
Control RNAi (n=15)
beta-catenin RNAi (n=11)
Control RNAi (n=14)
beta-catenin RNAi (n=11)
H
Total
Anterior
Posterior
p=0.091
p<0.0001
p<0.0001
Number of GCPs per brain width(cm)
Control RNAi (n=14)
beta-catenin RNAi (n=11)
Control RNAi (n=15)
beta-catenin RNAi (n=11)
Control RNAi (n=14)
beta-catenin RNAi (n=11)
I
Control RNAi (d39-41)
notum RNAi (d39-41)
lecg (pan-oocyte)
J
p=0.36
Number of ovaries per animal
Control RNAi (n=47)
notum RNAi (n=42)
K
p=0.37
Number of ovaries per brain length (cm)
Control RNAi (n=47)
notum RNAi (n=42)
L
p=0.28
Number of ovaries per brain width (cm)
Control RNAi (n=47)
notum RNAi (n=41)
M
p=0.37
Normalized ovarian distance (Do(n))
Control RNAi (n=164)
notum RNAi (n=176)
N
p=0.99
Maximum Do(n)
Control RNAi (n=45)
notum RNAi (n=43)
O
p=0.22
Minimum Do(n)
Control RNAi (n=45)
notum RNAi (n=43)
P
Total
p=0.59
Number of GCPs per ovary
Control RNAi (n=24)
notum RNAi (n=23)
p=0.019
Number of GCPs per brain length (cm)
Control RNAi (n=24)
notum RNAi (n=23)
p=0.0082
Number of GCPs per brain width (cm)
Control RNAi (n=24)
notum RNAi (n=23)
Q
<=30 um (Proximal)
p=0.42
Number of GCPs per ovary
Control RNAi (n=24)
notum RNAi (n=23)
p=0.74
Number of GCPs per animal
Control RNAi (n=24)
notum RNAi (n=23)
p=0.58
Number of GCPs per brain length (cm)
Control RNAi (n=24)
notum RNAi (n=23)
p=0.70
Number of GCPs per brain width (cm)
Control RNAi (n=24)
notum RNAi (n=23)
R
>30 um (Distal)
p=0.36
Number of GCPs per ovary
Control RNAi (n=24)
notum RNAi (n=23)
p=0.011
Number of GCPs per brain length (cm)
Control RNAi (n=24)
notum RNAi (n=23)
p=0.0063
Number of GCPs per brain width (cm)
Control RNAi (n=24)
notum RNAi (n=23)
S
Single Ovaries
Anterior Ovaries
Posterior Ovaries
p=0.031
p=0.27
p=0.0090
Number of GCPs anterior to each ovary per brain length (cm)
Control RNAi (n=19)
notum RNAi (n=14)
Control RNAi (n=14)
notum RNAi (n=11)
Control RNAi (n=14)
notum RNAi (n=13)
T
Single Ovaries
Anterior Ovaries
Posterior Ovaries
p=0.028
p=0.20
p=0.0021
Number of GCPs anterior to each ovary per brain length (cm)
Control RNAi (n=19)
notum RNAi (n=14)
Control RNAi (n=14)
notum RNAi (n=11)
Control RNAi (n=14)
notum RNAi (n=13)
U
lecg (pan-oocyte)
nhr-1 (tubas+oviducts)
Control RNAi (d39-41)
notum RNAi (d39-41)
V
p=0.78
% Disconnection
Control RNAi (n=20)
notum RNAi (n=18)
W
Anterior
Posterior
p=0.43
p=0.048
% Disconnection
Control RNAi (n=20)
notum RNAi (n=18)
Control RNAi (n=20)
notum RNAi (n=18)
X
Control RNAi (d39)
wnt5 RNAi (d39)
Control RNAi (d77)
wntA RNAi (d77)
lecg (pan-oocyte)

Figure S7. Additional information on ovarian phenotypes of Wnt-related RNAi conditions. Related to Figure 6.

(A) Quantification of the total number of ovaries per animal in control RNAi and *beta-catenin* RNAi-treated animals. Although there is no significant difference in the mean number of ovaries per animal between the two populations, the *beta-catenin* RNAi-treated animals have a more dispersed distribution of the number of ovaries than the control RNAi animals. P-values were computed using a Mann-Whitney U Test. **(B)** Quantification of the total number of ovaries per animal in control RNAi and *beta-catenin* RNAi-treated animals normalized to brain length. P-values were computed using Welch's T-Test. **(C)** Quantification of the total number of ovaries per animal in control RNAi and *beta-catenin* RNAi-treated animals normalized to brain width. P-values were computed using Welch's T-Test. **(D)** Quantification of the total number of ovaries per animal in control RNAi and *beta-catenin* RNAi-treated animals that possess at least one ectopic ovary normalized to brain length. P-values were computed using Welch's T-Test. **(E)** Quantification of the total number of ovaries per animal in control RNAi and *beta-catenin* RNAi-treated animals that possess at least one ectopic normalized to brain width. P-values were computed using Welch's T-Test. **(F)** Quantification of the average fluorescent area per ovary of oocyte (*lecg)* signal in control and *beta-catenin* RNAi-treated animals. P-values were computed using Welch's T-Test. **(G)** Quantification of the number of germ cell progenitors anterior to the ovaries (middle), posterior to the ovaries (right), and in total (left) normalized to brain length in control and *beta-catenin* RNAi-treated animals. P-values were computed using Welch's T-test. **(H)** Quantification of the number of germ cell progenitors anterior to the ovaries (middle), posterior to the ovaries (right), and in total (left) normalized to brain width in control and *beta-catenin* RNAi-treated animals. P-values were computed using Welch's T-test. This depletion in GCPs may result in the eventual loss of the ovaries, as observed in a fraction of the *beta-catenin* RNAi population. **(I)** Top: Representative widefield FISH images from control RNAi and *notum* RNAi-treated animals, showing the pan-oocyte marker *lecg* in green. (Bottom): Zoomed-in, confocal projections of *lecg* staining in the same ovaries. Scale bar=50 μm. **(J)** Quantification of the number of ovaries per animal in control and *notum* RNAi-treated animals. P-values were calculated using a Mann-Whitney U Test. **(K)** Quantification of the number of ovaries normalized to brain length in control and *notum* RNAi-treated animals. P-values were calculated using a Mann-Whitney U Test. **(L)** Quantification of the number of ovaries normalized to brain width in control and *notum* RNAi-treated animals. P-values were calculated using a Mann-Whitney U Test. **(M)** Quantification of the normalized ovarian distance for each ovary in control and *notum* RNAi-treated animals. P-values were calculated using a Mann-Whitney U Test. **(N)** Quantification of the maximum normalized ovarian distance (representing the posteriormost set of ovaries) for each ovary in control and *notum* RNAi-treated animals. P-values were calculated using Welch's T-Test. **(O)** Quantification of the minimum normalized ovarian distance (representing the anteriormost set of ovaries) in control and *notum* RNAi-treated animals. P-values were calculated using a Mann-Whitney U Test. **(P)** Quantifications of: (First): the total number of GCPs per ovary in control and *notum* RNAi-treated animals. P-values were calculated using Welch's T-Test. (Second): the total number of GCPs normalized to brain length in control and *notum* RNAi-treated animals. P-values were calculated using a Mann-Whitney U Test. (Third): the total number of GCPs normalized to brain width in control and *notum* RNAi-treated animals. P-values were calculated using a Mann-Whitney U Test. **(Q)** Quantifications of: (First): the number of proximal GCPs per ovary in control and *notum* RNAi-treated animals. P-values were calculated using Welch's T-Test. (Second): the number of proximal GCPs per animal in control and *notum* RNAi-treated animals. P-values were calculated using a Mann-Whitney U Test. (Third): the number of proximal GCPs normalized to brain length in control and *notum* RNAi-treated animals. P-values were calculated using a Mann-Whitney U Test. (Fourth): the number of proximal GCPs normalized to brain width in control and *notum* RNAi-treated animals. P-values were calculated using a Mann-Whitney U Test. **(R)** Quantifications of: (First): the number of distal GCPs per ovary in control and *notum* RNAi-treated animals. P-values were calculated using Welch's T-Test. (Second): the number of distal GCPs normalized to brain length in control and *notum* RNAi-treated animals. P-values were calculated using a Mann-Whitney U Test. (Third): the number of distal GCPs normalized to brain width in control and *notum* RNAi-treated animals. P-values were calculated using a Mann-Whitney U Test. **(S)** Quantification of the number of GCPs above single (left) anterior (center), and posterior (right) ovaries normalized to brain length in control and *notum* RNAi-treated animals. P-values were calculated using a Mann-Whitney U Test for the left panel, and Welch's T-Test for all other panels. **(T)** Quantification of the number of GCPs above single (left) anterior (center), and posterior (right) ovaries normalized to brain width in control and *notum* RNAi-treated animals. P-values were calculated using a Mann-Whitney U Test for the left panel, and Welch's T-Test for all other panels. **(U)** Representative sample maximum Z-projections of confocal stacks showing control (top) and *notum* RNAi-treated animals (bottom). Animals were stained for the pan-oocyte marker *lecg* to represent the ovaries in green and the oviduct and tuba marker *nhr-1* in magenta. Scale bar=50 μm. **(V)** Quantification of the percentage of ovaries lacking proper connections to either the oviducts or the tubas in control and *notum* RNAi-treated animals. P-values were calculated using a Mann-Whitney U Test. **(W)** Quantification of the percentages of anterior (left) and posterior (right) ovaries that lack proper connections to the tubas or oviducts in control and *notum* RNAi-treated animals. P-values were calculated using a Mann-Whitney U Test. **(X)** Preliminary sample widefield images of *wnt5* and *wntA* RNAi animals (right) taken at the indicated number of days post-treatment with time-matched controls (left) showing the pan-oocyte marker *lecg* in green. Scale bar=50 μm. Error bars of boxplots represent minimum and maximum observations. Solid lines on violin plots indicate medians, and dotted lines indicate quartile boundaries.

Gene Name	Gene ID [S3]	Primer Sequence (F)	Primer Sequence (R)	Target (FISH)	Application
Lecg	SMU15024371	TGCATCTATGAAAATCAGTGAAGG	TGCCAACATGGGAGTGGTTT	Oocytes	FISH
Nanos	SMU15028419	TTTTTCTCATGCGCACAGGC	AGAGTGGATTGTGACATGCTTCT	Germ cell progenitors	FISH
Ece-1	SMU15037788	AGTCGGAATTTGTTGATTGGTAAA	CCCACGGTTTGCAATGAAGG	Ovarian niche cells	FISH
Nhr-1	SMU15028438	TCGAGAGATGAAGGAGAAAAGAA	TTGCATGTGCCTGAAAGTGC	Oviducts+tubas	FISH
Notum	SMU15013569	TCCAAATCGTCTTGGTTCAGT	TGTTGAGTGTTCATTTTTCGCA	Anterior pole cells+testes	FISH+RNAi
Beta-catenin	SMU15031548	AACTTTTATGGACAGCTACGAGG	TCTATGGCTGACACATGGCG		RNAi
Dmd-1	SMU15013273	TCCACGGAATTGTGCTGGAA	TCGAAAATTAACGATTCTACCGGA		RNAi
Wnt1	SMU15027741	CGTCAATCATCTCAGAAACACCA	TGACATTCAACTTTGCAACACCA		RNAi
Wnt5	SMU15031231	GTGCTGCCGTGGAAAAATCA	CAGTCGAATGCAAACTTGGCA		RNAi
WntA	SMU15027091	TCGATGCTGGTATTGATTCTCAGA	TCGCATACAGCTTCAATCACA		RNAi
Gapdh	SMU15012454	TCTTCCCCAACCAATTTTCTGTTCTG	CCGAATATTTTATTTGGCTCTTCCTCCA		qPCR
Ubiquillin	SMU15020242	AAATTCGCCTGCCTGTTGGG	CCGGTGGCATTAATCCATCTGT		qPCR
Notum	SMU15013569	AGGTTTTGCAGCTCAGACTTTGA	ACACTAACATAAGCCCAATTACTTTTTGT		qPCR
Dmd-1	SMU15013273	TGTCCCACGGCTGTAAACCA	GCAGTTCGCTTTACGCTCAAAAC		qPCR
Wnt1	SMU15027741	GCTCAAACTGTCGCTGAGGC	CGTTGTCGTCACATCCTTGCC		qPCR
Wnt5	SMU15031231	ACAATGCTGGAAGAATGGCAGT	GGTGGCAACTGTTTCCAGCA		qPCR
WntA	SMU15027091	CATGTTGGAAGACAAGCGGTGA	AGGTAGAGCTCGAATGCACGT		qPCR

Table S1. Primer sequences used in this study. Related to STAR Methods.

Supplemental References

S1. Vila-Farré, M., Rozanski, A., Ivanković, M., Cleland, J., Brand, J.N., Thalen, F., Grohme, M.A., von Kannen, S., Grosbusch, A.L., Vu, H.T.K., et al. (2023). Evolutionary dynamics of whole-body regeneration across planarian flatworms. Nature Ecology & Evolution *7*, 2108-2124. 10.1038/s41559-023-02221-7.

S2. Chong, T., Collins, J.J., 3rd, Brubacher, J.L., Zarkower, D., and Newmark, P.A. (2013). A sex-specific transcription factor controls male identity in a simultaneous hermaphrodite. Nat Commun *4*, 1814. 10.1038/ncomms2811.

S3. Robb, S.M., Gotting, K., Ross, E., and Sánchez Alvarado, A. (2015). SmedGD 2.0: The Schmidtea mediterranea genome database. Genesis *53*, 535-546. 10.1002/dvg.22872.